NASA Technical Memorandum 102219

A Survey of Nonuniform Inflow Models for Rotorcraft Flight Dynamics and Control Applications

Robert T. N. Chen

November 1989

National Aeronautics and Space Administration

NASA Technical Memorandum 102219

A Survey of Nonuniform Inflow Models for Rotorcraft Flight Dynamics and Control Applications

Robert T. N. Chen, Ames Research Center, Moffett Field, California

November 1989

NASA

National Aeronautics and
Space Administration

Ames Research Center
Moffett Field, California 94035

A SURVEY OF NONUNIFORM INFLOW MODELS FOR ROTORCRAFT FLIGHT DYNAMICS AND CONTROL APPLICATIONS

Robert T. N. Chen

NASA Ames Research Center
Moffett Field, California 94035, USA

ABSTRACT

This paper summarizes the results of a brief survey of nonuniform inflow models for the calculation of induced velocities at and near a lifting rotor in and out of ground effect. The survey, conducted from the perspective of flight dynamics and control applications, covers a spectrum of flight conditions including hover, vertical flight, and low-speed and high-speed forward flight, and reviews both static and dynamic aspects of the inflow. A primary emphasis is on the evaluation of various simple first harmonic inflow models developed over the years, in comparison with more sophisticated methods developed for use in performance and airload computations. The results of correlation with several sets of test data obtained at the rotor out of ground effect indicate that the Pitt/Peters first harmonic inflow model works well overall. For inflow near the rotor or in ground effect, it is suggested that charts similar to those of Heyson/Katzoff and Castles/De Leeuw of NACA be produced using modern free-wake methods for use in flight dynamic analyses and simulations.

LIST OF SYMBOLS

a	Lift curve slope
A_{1c}	Lateral cyclic pitch
b	Number of blades per rotor
b_1	Lateral flapping angle
c	Blade chord length
C_l	Aerodynamic rolling moment coefficient
C_m	Aerodynamic pitching moment coefficient
C_T	Thrust coefficient
D	Rotor drag
F	Total force produced by the rotor (see Fig. 25)

$\bar{h}$ Ratio of rotor height above the ground to rotor diameter

H Distance of rotor above ground (see Fig. 25)

K Parameter in the static gain matrix relating the aerodynamic moments to the harmonic inflow components, K = 1 for a nonrigid wake, K = 2 for a rigid wake

K_c Ratio of cosine component to mean value of the first harmonic inflow, $K_c = v_c/v_0$

K_s Ratio of sine component to mean value of the first harmonic inflow, $K_s = v_s/v_0$

L Static gain matrix relating aerodynamic force and moments to the harmonic inflow components (also rotor lift, see Fig. 25)

M Apparent mass matrix associated with inflow dynamics

r Distance of blade element from axis of rotation

R Rotor radius

T Rotor thrust

Δu Ground-induced interference velocity in the tip-path plane

Δv Ground-induced interference velocity perpendicular to the tip-path plane

v Induced velocity at a general radial and azimuthal position (normalized with tip speed)

v_i = v, induced inflow ratio when normalized with tip speed

$v_{i,\infty}$ Induced velocity out of ground effect

v_z = –v (see Fig. 22, v_x = v)

v_0 Induced velocity at the rotor disc center, calculated by the momentum theory, $v_0 = C_T/[2(\mu^2 + \lambda^2)^{1/2}]$

v_c Cosine component of the first harmonic induced velocity, also denoted by λ_{1c}

v_s Sine component of the first harmonic induced velocity

v_h Mean induced velocity based on momentum theory at hover, $v_h = \sqrt{C_T/2}$

v_{HOV} Induced velocity at hover as a function of radial position

v_T Normalized total velocity at the rotor disc center, $v_T = (\mu^2 + \lambda^2)^{1/2}$

v_m Mass flow parameter, $v_m = [\mu^2 + \lambda(\lambda + v_0)]/v_T$

V_∞ Free-stream or flight velocity of the aircraft (normalized with tip speed)

V_v Vertical velocity of the aircraft

V_c Vertical climb velocity

$\overline{V}_c$ $= V_c/v_h$

V_d Vertical descent velocity (see Fig. 4)

w_0 $= -v_0$

Δw $= -\Delta v$

x $= r/R$

χ Wake skew angle, $\chi = \tan^{-1}(\mu/\lambda)$

μ Advance ratio, $\mu = V_\infty \cos \alpha$

μ^* Normalized advance ratio, $\mu^* = \mu/v_h$

α Tip-path plane angle of attack (also α_{TPP})

λ Inflow ratio, $\lambda = v_0 - V_\infty \sin \alpha$

λ_{1c} $= v_c$

Ω Rotor angular velocity

ψ Azimuth position

θ Blade pitch at radial position x

$\theta_{0.75}$ Blade pitch at radial position, x = 0.75

$*$ $= d/d\psi$ (see Eqs. (17), (19))

1. INTRODUCTION

This brief survey was undertaken with the intent of forming a basis for improving the aerodynamic representation of a generic helicopter mathematical model for real-time flight

simulation. As the dynamic representation of the rotor system reaches a given level of sophistication in terms of the applicable frequency range and of the degrees of freedom of the blade motion, it becomes apparent that a comparable level of detail must be used for its aerodynamic counterpart. At the heart of the helicopter aerodynamics are the induced velocities at and near the main rotor(s). In the past, uniform induced velocity has commonly been used to reduce computational burden in a real-time simulation environment because of limited computational capability in the simulation facility. With the rapidly expanding computational power at reduced cost in recent years, it has become possible to provide a more realistic representation of the inflow, accounting for its nonuniformity and the dynamics associated with the rotor wake. A cursory review of the current generation of rotorcraft models for real-time flight dynamic simulation indicates that some realism has been added in representing the inflow, but this has often been done in an ad hoc and empirical manner tuned for a specific rotorcraft.

This survey of inflow models covers a spectrum of flight conditions including hover, vertical flight, and low-speed and high-speed forward flight. Both static and dynamic aspects were reviewed, both in and out of ground effect. With real-time applications in mind, a main focus of the survey was placed on the comparative evaluation of several simple first-harmonic inflow models using available old and new test data. In particular, the wind tunnel data obtained recently by Elliott and Althoff [1] with a laser velocimeter was used for correlation. Hoad et al. [2] did extensive correlations of these data with predictions from several state-of-the-art analytical rotor wake calculation methods. The survey provides, therefore, a good opportunity to determine how well the simple first harmonic inflow models perform compared to the advanced wake models.

2. A BRIEF HISTORICAL PERSPECTIVE

In 1926, Glauert [3], in trying to resolve discrepancies between the experimentally observed and theoretically calculated lateral force of the rotor from uniform inflow, proposed a simple first harmonic nonuniform inflow model which generates an induced velocity field

$$v = v_0(1 + xK_c \cos \psi) \tag{1}$$

that increases longitudinally from the leading edge to the trailing edge of the rotor disc with the gradient K_c being unspecified. Wheatley [4] correlated a preselected value of the gradient ($K_c = 0.5$) with flight-test data that he gathered from an autogyro. One of his conclusions was that "the blade motion is critically dependent upon the distribution of induced velocities over the rotor disc and cannot be calculated rigorously without the accurate determination of the induced flow." Seibel [5] explained that it is the nonuniform inflow that causes the "hump" of the vibratory load which was encountered in the low-speed flight regime during flight-testing of the Bell Model 30. To better define the induced velocities over the rotor disc for further vibration study, Coleman et al. [6] in 1945 introduced a simplified vortex system of the rotor (a cylindrical wake model) and used it to develop an analytical formula for the normal component of induced velocity along the fore and aft diameter of the rotor disc. They also arrived at a remarkably simple formula for the gradient of the induced velocity at the rotor disc center, which is expressed in terms of wake skew angle (as defined in Fig. 1), as

$$K_c = \tan(\chi / 2) \tag{2}$$

Thus for the first time the value of K_c, left largely unspecified by Glauert, was analytically determined. Later, Drees [7] determined K_c using a wake geometry modified from Coleman's simple cylindrical vortex wake to account for the bound circulation varying sinusoidally with azimuth. When expressed in terms of the wake skew angle, Drees' formula for K_c yields

$$K_c = \frac{4}{3}(1 - 1.8\mu^2)\tan\frac{\chi}{2} \tag{3}$$

which shows that the gradient is a function of both the wake skew angle, χ, and the advance ratio, μ.

In 1947, Brotherhood [8] conducted a flight investigation of the induced velocity distribution in hover, and showed that flight-test measurements correlated well with values calculated using blade-element momentum theory [9,10]. Later, Brotherhood and Steward [11] also reported their flight-test work in forward flight using smoke filaments to indicate the flow pattern. They estimated that the value of the gradient K_c was between 1.3 and 1.6 in the range of advance ratios tested (0.14 to 0.19), thereby concluding that Eq. (2), derived by Coleman, tended to substantially underestimate the value of K_c. They also showed that the theoretical calculation of Mangler and Square [12] based on potential theory did not correlate well with their flight-test measurements of the induced velocities.

Up to the early 1950s, all the research on the induced velocity of the lifting rotor had been focused on the static or time-averaged aspect. In 1953, Carpenter and Fridovich [13] proposed a dynamic inflow model to investigate the transient rotor thrust and the inflow buildup during a jump takeoff maneuver. They extended the simple momentum theory for steady-state inflow to include the transient inflow buildup involving the apparent air mass that participates in the acceleration. The results of the calculation using the model were in good agreement with the experimental data obtained on a helicopter test stand. Unfortunately, research on the dynamic aspect of the induced velocity was not pursued further until two decades later. Meanwhile, work continued on the refinement of the static aspect of the theory of induced velocities at and near the lifting rotor.

A concerted effort was carried out at NACA during the 1950s to further develop the simple vortex theory introduced by Coleman et al. [6]. The work of Castles and De Leeuw [14] on the induced velocity near a uniformly loaded rotor, and the work of Heyson and Katzoff [15] for nonuniformly loaded rotors, culminated in the NACA charts [16] which are still used in the helicopter industry today, particularly in the flight mechanics discipline. With the increasing digital computational power that became available in the 1960s, sophisticated computer codes (e.g., [17,18]) were developed using more complicated prescribed helical-wake models. Work on free-wake codes was also begun (e.g., [19,20]) during the late 1960s and early 1970s. Heyson [21] and Landgrebe and Cheney (see Ref. 77) provided excellent reviews of the research activities on static inflow modeling using vortex theory in the U.S. during this period. Reference 77 also discussed the inherent capability of the transient inflow

calculation using free-wake methods. Some of the activities in the U.S.S.R. during these years are summarized in Refs. 22 and 23.

In 1972, Harris [24] published a set of low-speed flapping data obtained from a well-controlled wind tunnel test. He correlated calculated flapping angles using various static inflow models, including Coleman's model [6], NACA charts, and a representative prescribed helical-wake computer code [18], then available with his experimental data. He found that none of the available methods was able to predict lateral flapping in the low advance ratio region as shown in Fig. 2. The existence of a strong first-harmonic longitudinal component, as evident from Fig. 2, causes a variety of undesirable rotorcraft characteristics such as noise and vibration in the low-speed flight regime as mentioned earlier [5], and a large stick migration with speed and load factor, which may cause a loss of control for rotorcraft. Ruddell [25] reported that the value for Glauert longitudinal inflow gradient, K_c, used in the design calculation for cyclic control of the first advancing-blade-concept (ABC) aircraft was found to be much less than the actual value derived from flight tests. This discrepancy resulted in the loss of control which caused the 1973 ABC accident. In his work, Harris [24] suggested that, to achieve an improved correlation with his experimental data, free-wake rather than prescribed-wake approaches should be pursued. His suggestion was finally realized in 1981 by Johnson [26] with his comprehensive CAMRAD [27] computer code, which uses the Scully [28] free-wake analysis. With some tuning of a parameter (tip vortex core radius), Johnson was able to correlate very well his calculated lateral flapping with Harris' experimental data. Work is continuing (e.g., [29,30]) by the rotorcraft aerodynamicists in improving free-wake codes with respect to model fidelity and computational efficiency for applications directed primarily toward performance and airload calculations. As might be expected, free-wake codes are, in general, very computationally intensive.

For flight dynamics and control applications, a simple harmonic, finite-state, nonuniform inflow model for induced velocity similar to that originally proposed by Glauert is still being used extensively [31-34]. This form of model is easier to use and the results are easier to interpret in a nonreal-time environment. It is the only practical nonuniform inflow model that is not computationally intensive and thus can be implemented on a current-generation digital computer for real-time simulation. In 1971, Curtiss and Shupe [35] extended Glauert's model to include inflow perturbations from pitching and rolling moments, using the simple momentum theory. A similar first harmonic inflow model was also developed using a simple vortex theory by Ormiston and Peters [36]. Building upon the work of Curtiss and Shupe and using the concept of inflow dynamics introduced by Carpenter and Fridovich [13], Peters [37] developed, based on momentum theory, a more complete dynamic inflow model for hover. Dynamic inflow models for hover similar to that of Peters were also proposed by Crews, Hohenemser, and Ormiston [38], Ormiston [39], and Johnson [40,41]. Peters' dynamic inflow model was validated with wind tunnel data [42,43] using system identification methods. Using unsteady actuator disc theory, Pitt and Peters [44] extended Peters' [36] model for hover to include forward flight conditions, thereby completing the three-state, first harmonic, perturbed dynamic inflow model that has found broad applications in rotorcraft dynamics. For flight dynamic simulations, it was found [e.g., 45] that nonlinear dynamic inflow models such as that of Carpenter and Fridovich [13] and Peters [46,47], in lieu of the linear version

[44], are often the most suitable form to use, because total values, rather than the perturbed values, of the thrust and the pitching and rolling moments are involved.

In this paper, a main focus is on review and comparative evaluation of several first harmonic inflow models that have been developed since the work of Harris in 1972. In addition to the assessment of their steady-state effects as examined by Harris [24,48], the significance of the low-frequency, unsteady wake effects (inflow dynamics) is also addressed. First, for the static case, the Blake/White model [49], which was developed in 1979 from a simple vortex theory is compared with the steady-state solution of the Pitt/Peters dynamic inflow model [47], the classical Coleman model [6], and an inflow model used by Howlett [31], which represents current practice in real-time simulation of rotorcraft using a blade-element method. Inclusion of airmass dynamics associated with a lifting rotor have been shown recently by Curtiss [32], Miller [50], Chen and Hindson [45], and Schrage [34] to be important in the design of high-bandwidth flight-control systems for rotorcraft because the frequencies of the inflow dynamic modes are of the same order of magnitude as are those of the rotor-blade flapping and lead-lag modes. Therefore, the paper will also discuss dynamic inflow models that account for unsteady wake effects. Table 1 summarizes the events related to the development of some inflow models.

3. INFLOW MODELS—STATICS

Since this survey of inflow models is from the perspective of the user in flight dynamics and control, the inflow models of interest will be a function of the frequency range of applicability and will have an accuracy consistent with the applications for which a specific flight dynamics mathematical model is intended. For low-frequency applications (less than 0.5 Hz), such as trim computations or flying-qualities investigations involving low-bandwidth maneuvering tasks, the dynamic effects of the interaction of the airmass with the airframe/rotor system may be expected to be negligible, and therefore static inflow models will be of interest. The static characteristics of the induced velocity of a lifting rotor depend strongly on the operating conditions: hovering, vertical ascent or descent, low-speed forward flight, or high-speed cruise. For each of these flight regimes, some physical description and the associated mathematical models, with experimental correlation where available, are reviewed below. Ground effects of the rotor that are important for low-speed and low-level flights are reviewed, and induced velocities near the lifting rotor which are required for calculations of forces and moments for other parts of the airframe are discussed. Static characteristics resulting from rotor thrust will be addressed first, and then the influence of the pitching and rolling moments of the rotor system on the inflow distribution will be discussed.

3.1 Static Effect of Thrust

A. Hover and Vertical Flight

Out of Ground Effect. The flow patterns at and near the rotor in hover and in vertical flight were investigated extensively in the 1940s and 1950s, both analytically and experimentally. Figure 3, from Ref. 10, illustrates the flow patterns and the normalized induced velocity in terms of rate of climb, V_c, in vertical flight out of ground effect . A more detailed description

Table 1. Nonuniform Inflow Model Development—Flight Mechanics Perspective

Year	Author(s)	Remarks
1926	Glauert	Proposed a "triangular" induced velocity model: $v(r/R,\psi) = v_0[1 + (r/R)K_c \cos \psi]$.
1934	Wheatley	Used $K_c = 0.5$ to correlate with flight data; found inadequate in predicting flapping.
1944	Seibel	Explained that the severe vibration "hump" at low speeds encountered in flight tests of Bell Model 30 is caused by the nonuniform inflow.
1945	Coleman et al.	Determined that $K_c = \tan(\chi/2)$, using a vortex theory with a uniformly loaded circular disk (χ = wake-skew angle).
1949	Drees	Determined K_c using a wake geometry modified from Coleman's (assuming bound circulation varies sinusoidally with azimuth).
	Brotherhood et al.	Conducted a flight test using smoke filaments to indicate the flow pattern; estimated $K_c = 1.3$ to 1.6 in the μ range of 0.14 to 0.19.
1950	Mangler/Square	Developed induced velocity contours for lighted, nonuniformly loaded rotors for several values of TPP angle of attack.
1953	Carpenter/Fridovich	Developed inflow dynamics with respect to thrust variations.
1953 to 1959	Castles/DeLeeuw; Heyson/Katzoff/Jewel	Developed NACA charts of induced velocities near uniformly and nonuniformly loaded lifting rotors.
1959 to 1967	Miller; Piziali/DuWardt; Davenport et al.	Developed computer codes for various prescribed-wake models.
1967 to present		Development of free-wake codes such as UTRC codes and CAMRAD.

Table 1. Continued

Year	Author(s)	Remarks
1971	Curtiss/Shupe	Developed equivalent Lock number to account for inflow variations w.r.t. aerodynamic pitching and rolling moments.
1972	Harris	Correlated several inflow models with his wind tunnel data and found that none were able to predict the lateral flapping at low advance ratio ($\mu < 0.15$).
1974	Peters	Developed a more complete inflow model for hover based on momentum theory.
1976	Ruddell	Documented that value of the Glauert gradient term, K_C, used in the design calculation for cyclic control of the first ABC aircraft was much less than actual value, resulting in accident in 1973.
1977 to 1979	Banerjee/Crews/ Hohenemser	Identified the dynamic inflow parameters using wind tunnel data.
1979	Blake/White	Determined, using a simple vortex theory, the value of $K_C = \sqrt{2} \sin \chi$.
	Van Gaasbeek	Documented the inflow model used in the modern version of C-81 code, based on Drees' data.
1981	Johnson	Used free-wake (Scully wake) in CAMRAD to achieve good correlation with lateral-flapping data of Harris (1972).
	Pitt/Peters	Developed a complete dynamic inflow model for forward flight using unsteady actuator disk theory.
	Howlett	Documented the inflow model used in GENHEL-Black Hawk Engineering Simulation model.
	Junker/Langer	Obtained downwash measurements at low advance ratios from three tunnels and correlated them with calculations from local-momentum and rigid-wake theories.

Table 1 Concluded

Year	Author(s)	Remarks
1986	Chen/Hindson	Investigated effects of dynamic inflow on vertical response in hover using Carpenter and Pitt models and CH-47 flight data.
1987	Harris	Provided a historical perspective of static nonuniform inflow development—an update of his 1972 work.
1988	Hoad/Althoff/Elliott	Correlated several prescribed-wake and free-wake models with their recent tunnel-measured inflow data (from a laser velocimeter); showed poor agreement.
	Cheeseman/Haddow	Measured (using hot wire probes) downwash at low advance ratios; estimated value of K_c to be about 50% higher than Coleman's value.
	Peters/HaQuang	Refined nonlinear version of Pitt/Peters dynamic inflow model for practical applications.

can be found in Refs. 51 and 52. The momentum theory is applicable in the propeller working state, but only in portions of the regions of the windmill brake state and the vortex ring state. In the regions where the momentum theory is applicable, the mean value of the induced velocity can be calculated as shown in Fig. 3. In this figure, the mean induced velocity at the the tip-path plane (TPP) of the rotor and the vertical flight speed are normalized by the mean value of the induced velocity at hover, $v_h = \sqrt{C_T / 2}$, thereby removing their dependency on the air density and the disc loading. An empirical curve is indicated for the flight conditions where the momentum theory is no longer applicable because a well-defined slipstream does not exist. Within the region where the slipstream exists, it contracts or expands rapidly to reach a fully developed wake. The radius of the fully developed wake can be calculated by using the fully developed induced-velocity and continuity condition [23], as shown in Fig. 4. Note that the contraction ratio is 0.707 in hover, as shown. A recent calculation by Bliss et al. [53] using a free-wake analysis involving a three-part wake model (Fig. 5) indicated that the contraction ratio at the fully developed wake in hover is somewhat larger than that calculated using momentum theory. This is shown in Fig. 6, where a similar trend is also indicated for an empirical wake, as developed in Ref. 54.

The induced velocity at the rotor plane is nonuniform. Measurements from flight by Brotherhood [8] are shown in Fig. 7, in which calculations using blade-element momentum theory [9] and uniform inflow are also shown. The measurements were taken at two planes, 0.073R and 0.39R, below the rotor TPP, and the induced velocity at the rotor was then

extrapolated using stream lines obtained from smoke photographs. Thus, the measured data near the blade tip may not be accurate. Nevertheless, it can be seen from Fig. 7 that, except for the few percent of the rotor radius near the blade tip region, the induced velocity in hover calculated from blade-element momentum theory [9],

$$v = \left(\frac{V_v}{2} + \frac{bca\Omega}{16\pi}\right)\left[-1 + \sqrt{1 + \frac{2\Omega r(\theta - V_v/\Omega r)}{\left(4\pi V_v^2/bca\Omega\right) + V_v + (bca\Omega/16\pi)}}\right] \tag{4}$$

correlates very well with flight-measured data. Near the blade tip, large variations in induced velocity are caused by the strong influence of the contracted tip vortex. However, calculations of the distribution of the induced velocity near the blade tip based on vortex theory are sensitive to tip vortex geometry [55]. As shown in Fig. 8, Landgrebe [56] calculated the hover-induced velocity distribution using several prescribed wake models and compared the results with those from the blade-element momentum theory. Free-wake methods, though promising, have yet to achieve a level of accuracy permitting their routine use in performance calculations [48]. Generally, however, an accuracy level somewhat less than that required for performance estimation is sufficient for stability and control analysis. Equation (4) is therefore a good approximation for simple nonuniform inflow, out of ground effect, at the rotor blade for low-frequency applications in flight dynamics and control.

A knowledge of induced velocity near the lifting rotor is required for the calculation of the forces and moments acting on the fuselage, the tail rotor, and the horizontal and vertical tails. Examples of NACA charts [16], for which calculations were made using a simple cylindrical wake with (1) uniform disc loading and (2) a triangular disc loading at hover, are shown in Fig. 9. Improvements using free-wake methods presented in a similar chart form, or in look-up tables for various geometrical characteristics and operating conditions of a lifting rotor, are presently lacking. These are needed for rapid calculations in flight dynamics and control simulations, especially for real-time applications.

Effect of Ground. In ground proximity, the induced velocity decreases, since in the ground plane the vertical airspeed component must be zero. The effect of the ground on the mean induced velocity as determined by model and full-scale tests can be found, for example, in Ref. 57. As is well known, the ground effect becomes negligible when the height of the rotor plane above the ground is larger than the diameter of the rotor. The induced velocity distribution along the rotor blade was calculated many years ago by Knight and Hefner [58] using a simple cylindrical vortex wake for a uniformly loaded rotor disc and the method of images, as shown in Fig.10. Note that without the effects of the ground, the induced velocity distribution is uniform, and is identical to that shown in Fig. 9a for the uniform disc-loading case. Nonuniformity increases as a result of the ground effect as the rotor disc approaches the ground plane. Ground-induced interference velocities are largest at the rotor center and smallest at the blade tip. However, the disc-load distribution can have significant effects on the distribution of ground-induced interference velocities over the rotor disc. Heyson [59] has calculated and compared the uniform and triangular disc-load distributions, as shown in Fig. 11. The interference is nonuniform in spanwise distribution, particularly for the

triangular disc-load distribution for low values of the rotor height above the ground. The large distortion near the rotor center is a result of the zero load at the rotor center for the triangular disc-load distribution. The induced-velocity distribution at the rotor disc can then be obtained by combining the information in Fig. 11 with corresponding out-of-ground-effect (OGE) values at the rotor disc in Figs. 9a and 9b. Note that for uniform disc-load distribution, the result is identical to that shown in Fig. 10, as it should be. In Ref. 59, Heyson also provided some of his calculations of the flow field of a triangularly loaded rotor in ground proximity, which may be compared directly with its OGE counterpart in Fig. 9b to gain qualitative insight into the ground effect. Because of the failure to consider wake distortions in the prescribed simple cylinder wake method, a high level of accuracy cannot be expected. A systematic correlation of these results with those calculated using the more sophisticated free-wake methods, and with test data to quantify the degree of accuracy of the calculated results, has also been lacking.

B. Low-Speed Forward Flight

Out of Ground Effect. As the forward speed increases from hovering, the rotor wake is swept rearward. The wake skew angle (see Fig. 1) increases rapidly from 0° in hover to 90° in edgewise flight, and at the same time the mean induced velocity decreases. The wake skew angle and the mean induced velocity can be calculated for various values of TPP angle of attack, using the uniform induced velocity formula proposed by Glauert [3], based on the momentum theory,

$$v_0 = C_T / 2(\mu^2 + \lambda^2)^{1/2} \tag{5}$$

and the definition of the wake skew angle,

$$\tan \chi = \mu / \lambda \tag{6}$$

where $\mu = V_\infty \cos \alpha$, $\lambda = v_0 - V_\infty \sin \alpha$ (note that V_∞ is normalized with tip speed). Figure 12 shows the wake skew angle as a function of the normalized flight velocity (normalized with respect to the hover uniform induced velocity, v_h) for several values of TPP angle of attack. At a given flight velocity the wake skew angle is considerably larger in descending flight (positive values of α) than in climbing flight (negative values of α). Note that at zero TPP angle of attack, the wake skew angle already reaches about 80° at the normalized flight speed of about 2.3 (corresponding to $\mu = 1.62\sqrt{C_T}$). The calculated wake skew angles for the smaller values of α correlate well with measured data, as shown in Fig. 13 [10]. Similarly, the calculated mean induced velocity at low speeds using Eq. (5) matches fairly well with the measured values.

The wake skew angle, which is dependent upon advance ratio, TPP angle of attack, and thrust coefficient, defines the orientation of the rotor wake and is a key parameter in determining the induced velocity at and near a lifting rotor. Figure 14 shows the contours of induced-velocity ratio v/v_0 in the longitudinal plane of the rotor for various wake skew angles. These were calculated by Castles and DeLeeuw [14] using a cylindrical wake with uniform disk loading, and they show that the induced velocity at the rotor plane is strongly

dependent on the wake skew angle. Payne has suggested [51] that the results of Castles and DeLeeuw may be approximated by a first-harmonic expression similar to that originally proposed by Glauert:

$$v = v_0 + x(v_c \cos \psi + v_s \sin \psi) \tag{7a}$$

$$= v_0[1 + x(K_c \cos \psi + K_s \sin \psi)] \tag{7b}$$

where $v_0 K_c = v_c$, $v_0 K_s = v_s$, and

$$K_c = \frac{(4/3)\tan \chi}{1.2 + \tan \chi} \tag{8}$$

and $K_s = 0$. Over the years several authors have developed other formulae for K_c and K_s. Some of these, recast as an explicit function of wake skew angle, are summarized in Table 2.

Table 2. First Harmonic Inflow Models

Year	Author(s)	K_c	K_s
1945	Coleman et al. [6]	$\tan(\chi/2)$	0
1949	Drees [7]	$(4/3)(1-1.8\mu^2)\tan(\chi/2)$	-2μ
1959	Payne [55]	$\frac{(4/3)\tan \chi}{1.2+\tan \chi}$	0
1979	Blake and White [49]	$\sqrt{2} \sin \chi$	0
1981	Pitt and Peters [44]	$(15\pi/32)\tan(\chi/2)^a$	0
1981	Howlett [31]	$\sin^2 \chi$	0

[a]Considering only static and with only thrust effect.

A comparison of the ratio of the cosine component to the mean induced velocity for several models listed in Table 2 is shown in Fig. 15 as a function of the wake skew angle.

With the wake skew angle calculated as shown in Fig. 12, a comparison of the cosine component of the induced velocity from those models listed in Table 2, at various flight conditions, can be made. Figure 16 shows such a comparison for those inflow models shown in Fig. 15 for climbing, level flight, and descending flight conditions. As the flight speed increases, the cosine component of the induced velocity peaks at a flight speed less than twice the hover uniform induced velocity. Thus, the flight speed at which the cosine component of the induced velocity peaks depends on the thrust coefficient at which the rotor is operating, with a higher flight speed for a higher thrust coefficient. The peak amplitude also

depends strongly on the sign of the TPP angle of attack; it is larger when the value of α is positive, as in a descending flight or in a flare, than when the value of α is negative, as in a level or a climbing flight. These trends are consistent with the vertical vibration level in low-speed flights typically observed by the pilot or measured in flight, as shown in Figs. 17 and 18 (taken from Refs. 60 and 61, respectively). As mentioned earlier, some general characteristics of the low-speed vibration due to the fore-and-aft variation in the induced velocity were investigated by Seibel [5] many years ago. With the emphasis on nap-of-the-Earth (NOE), low-speed terrain flying in recent years for military missions, interest has resumed in a thorough reexamination of the vibration problem associated with low-speed maneuvering flight.

In Fig. 16, it is seen that as the flight speed increases beyond the peak of the cosine component of the induced velocity, both the mean and the cosine component of the induced velocity diminish rapidly, reducing their impact on the rotor forces and moments. In the peak region, the magnitude of the cosine component varies significantly among the models, being much larger for the Blake/White and Pitt/Peters models than for the classical model of Coleman et al. [6]. Cheeseman and Haddow [62] recently gathered induced-velocity data at low advance ratios from a wind tunnel, using triaxial hot-wire probes. They compared the values of the longitudinal inflow gradient, K_c, fitted from the measured inflow data with those calculated from Coleman's model, and found that the calculated values were 45% to 56% smaller, depending on the flight conditions, than the measured values, as shown in Table 3. For a broader comparison, some of the first harmonic inflow models listed in Table 2 are also included in Table 3. The results show that the Pitt/Peters inflow model correlates best with the Cheeseman-Haddow data, differing by only 2% to 7% from their fitted experimental data. The Drees model and the Payne model also match the data fairly well, differing by 10% to 16% from the fitted values, depending on the operating conditions. Some improvements of other models (e.g., Blake and Howlett) over the classical Coleman model can also be seen in Table 3.

The Cheeseman/Haddow data were obtained for small values of TPP angle of attack (about $-1.75°$). To see the potential effect of the TPP angle of attack, Fig. 16 was replotted for K_c, as shown in Fig. 19. It can be seen that the value of K_c tends to be higher for a positive value of α than for a negative value of α. For the $\alpha = 20°$ case, the K_c values for the four inflow models peak at flight speeds below $V_\infty/v_h = 2$, when the wake skew angle exceeds 90°.

An indirect means of estimating K_c is through correlations of the calculated lateral flapping values with those measured. As described earlier, Harris [24] has done such a correlation, as shown in Fig. 2. The Blake/White model achieved a fairly good correlation with the Harris wind tunnel data, as shown in Fig. 20 [63]. In 1987, Harris [48] expanded his 1972 work [24] to include correlations of the (1) Blake/White model [49]; (2) the Scully free-wake model used in the CAMRAD [26]; and (3) the inflow model used in the C-81 [64], which was developed empirically based on Drees' model together with his low-advance-ratio data obtained from a wind tunnel. The results, shown in Figs. 21 and 22, again indicate that the Blake/White simple model agrees fairly well with Harris' experimental data, and in the longitudinal plane of symmetry, the induced velocity compares well with that calculated from

Table 3. Comparison of Some First-Harmonic Inflow Models with Cheeseman Haddow Wind-Tunnel Data

Parameter	Test condition		
	1	2	3
Advance ratio	0.1	0.067	0.067
Rotor rpm	2500	2500	1250
	K_c		
Fitted from measured data [62]	1.07	0.96	0.92
Coleman et al.	0.74	0.61	0.59
Pitt/Peters	1.09	0.90	0.87
Howlett	0.92	0.79	0.77
Blake/White	1.35	1.26	1.24
Drees	0.96	0.81	0.78
Payne	0.98	0.82	0.80

CAMRAD. Harris noted, however, that the Blake/White model did not agree well with the other set of data that he used [48].

Another indirect method of estimating K_c at low speeds is by examining the cyclic control requirements for trim, since lateral cyclic inputs are required to trim out the rolling moment generated from the lateral flapping discussed above. Faulkner and Buchner [65] reported that, for a hingeless rotor helicopter, the Blake/White model generally yielded better results than the Payne model did. Ruddel [25] indicated that use of a K_c value similar to that of Coleman's in the design analysis was found to be about a factor of two too small in predicting the required cyclic control for trim (Fig. 23). The Cheeseman/Haddow data discussed earlier tend to corroborate this result.

In Ground Effect. With the emphasis on NOE flight in some operational missions, research in rotor aerodynamics in ground proximity at low advance ratios has been reactivated in recent years. As the forward speed increases, the wake of the rotor is rapidly swept rearward, and as a result, the effect of the ground is rapidly reduced. Without the ground effect, it can be seen in Fig. 12 that the wake skew angle has already reached approximately 75° at a flight speed twice the hover mean induced velocity (for zero TPP angle of attack). An early study [66] using a cylindrical wake model with the method of images indicates that, for zero TPP angle of attack, the ground effect virtually disappears at speeds greater than twice the hover mean induced velocity, as illustrated in Fig. 24. The normalized induced velocity at the rotor center is plotted as a function of the normalized forward speed for various values of rotor height above the ground. Note that for $Z/R = \infty$, the curve, which is monotonically decreasing, is identical to that out of ground effect as shown in Fig. 16 ($\alpha = 0$). For smaller values of Z/R, the total induced velocity at the center of the rotor increases rather than decreases as the flight speed increases, because the decrease in ground effect with speed is more rapid than the decrease in induced velocity in forward flight. Although the simple vortex theory used in

Ref. 66 does not include such effects as ground vortex, similar phenomena have been observed in flight [67] and in wind tunnel tests [68,69]. Formation of the ground vortex in the region of very low advance ratios ($u < 0.06$), which was observed by Sheridan [68], was attributed to the increase in power required, in that flight regime, for rotor heights less than about one-half of the rotor radius.

In ground proximity, the OGE mean induced velocity and wake skew angle, Eqs. (5) and (6), according to momentum theory, require modifications to account for the vertical and horizontal components, Δv and Δu, of the ground-induced velocity (see Fig. 25). It can be shown [59] that

$$(v_0 / v_h)^4 = \frac{1}{[(V_\infty / v_0) + \tan\alpha - (\Delta u / v_0)]^2 + [1 + (\Delta v / v_0)]^2} \tag{9}$$

and

$$\cos\chi = (v_0 / v_h)^2 [1 + \Delta v / v_0] \tag{10}$$

In computing the ground-induced interference velocity, wake roll-up must to be considered. Observations have indicated that the roll-up of the wake takes place rapidly behind the rotor, similar to a low-aspect-ratio wing, as shown schematically in Fig. 26. Using an analogy to an elliptically loaded wing, Heyson [59] proposed to use an effective skew angle which is related to the momentum wake skew angle by

$$\tan\chi_e = (\pi^2 / 4)\tan\chi \tag{11}$$

for the calculation of the ground effect in forward flight. (Note that the effective wake angle is considerably larger than the momentum skew angle in the region of low values of χ.) A sample of results calculated [59] using the skewed cylinder wake with the method of images is shown in Fig. 27 for the distribution of the vertical component of ground-induced interference velocity at $\chi_e = 30°$, 60°, and 90°. As in the hover case, the results are sensitive to the disc-load distribution in the low-rotor-height region. Since the disc-load distribution is generally not known beforehand, the results are not very useful. Another shortcoming of the analysis is the failure to consider the distortion of the near wake resulting from the influence of the ground and of the roll-up wake. Here, free-wake methods may play an important role. Sun [70] recently developed a simplified free-wake/roll-up-wake flow model to investigate the aerodynamic interaction between the rotor wake, the ground, and the roll-up wake and to calculate the induced-velocity distribution at the rotor plane. He found that the near-wake deformation from the influence of the ground and the roll-up wake causes large variations in the induced-velocity distribution near the blade tip in the forward part of the rotor. After a proper calibration with test data, plots similar to NACA charts [16] for OGE are needed for IGE to be used in detailed flight-dynamic simulations, particularly in a real-time environment as either look-up tables (similar to those used in Ref. 71) or simple curve-fit equations (similar to those used in Ref. 72).

For flight-dynamic simulations, first-harmonic inflow models, either in static [71] or dynamic [32-34] form, have been used in recent years. Curtiss [73] recently analyzed and determined effective values of the constant and first-harmonic inflow coefficients, v_0, v_c, and v_s, in Eq. (7a), using low-advance-ratio ground-effect data obtained from the Princeton Dynamic Model Track facility [70,74]. The experimental facility and the model rotor are described in Refs. 73 and 74. Some of these obtained by Curtiss, recast in the format of Fig. 16, are shown in Figs. 28 and 29. Figure 28 shows an example of the value of v_0/v_h vs. V_∞/v_h at $Z/R = 0.88$. The value calculated from the momentum theory, OGE, which is identical to that shown in Fig. 16 ($\alpha = 0$), is also plotted (shown by the dashed line) for comparison. When the value of the normalized speed, V_∞/v_h, is less than about 1, the effect of the ground is favorable in that it reduces the mean induced velocity to a value below that indicated by the momentum theory. However, the effect of the ground becomes adverse when the value of the normalized speed, V_∞/v_h, is increased beyond 1. These experimentally derived characteristics are considerably different from those obtained from the simple vortex theory of Heyson [59] shown in Fig. 24, in which the effect of ground is always favorable.

Curtiss [73] also found from the experimental data that the effect of the ground is to reduce significantly the cosine (the fore-and-aft) component of the harmonic inflow. As shown in Fig. 29, the normalized cosine component is depicted as a function of height-to-radius ratio at two collective pitch settings. For purposes of comparison, values calculated using the Blake/White theory [49], which is one of the four OGE theories shown previously in Fig. 16, are also plotted in the figure. As shown, an increase in collective pitch somewhat decreases the value of the normalized cosine component at the higher values of the normalized flight speed. At low speeds, the recirculation may prevent the development of a longitudinal distribution of the induced velocity. The flow field in this flight regime is extremely complicated. Flow-visualization experiments [70,74] indicated that there are two distinct flow patterns: recirculation and ground vortex, as shown in Fig. 30. From hover to the normalized advance ratio of about 0.5, depending on the rotor height, is the region of recirculation of the wake through the rotor. As the speed is increased, a new pattern in the form of a concentrated vortex appears under the leading edge of the rotor. These experiments also indicated that the induced velocity is very sensitive to low levels of translational acceleration and deceleration. The sine component (or lateral distribution) of the induced velocity was found to be negligible in this very-low-speed flight regime (advance ratio <0.1).

C. High-Speed Forward Flight

When the forward speed increases beyond the normalized speed, $V_\infty/v_h = 2$, the mean induced velocity will decrease by more than 50% of the hover value and the wake skew angle (for $\alpha = 0$) will exceed 75°. In this flight regime, therefore, the effect of the ground disappears, and the influence of the induced velocity on the rotor forces and moments becomes less significant. Nevertheless, it is of interest to review some of the work related to this flight regime, and to show how some of the simple first-harmonic inflow models listed in Table 2 correlate with some of the old and new experimental data. Applicable theories for the calculation of inflow near the rotor in this flight regime, which provide a method for estimating the resulting forces and moments acting on the tail rotor and tail surfaces, will also be reviewed briefly.

In 1954, Gessow [10] provided an excellent survey of work on the induced flow of a lifting rotor. He showed by an example that in high-speed forward flight, the induced velocity distribution at the rotor disc calculated from the simple cylindrical wake model of Castles and DeLeeuw [14] correlated fairly well with that derived from smoke-flow pictures obtained in flight by Brotherhood and Steward [11]. Gessow's example is shown in Fig. 31. Note that in the figure, the normalized induced velocity, v/v_h, is equal to $(v/v_0)(v_0/v_h)$. Thus, the calculated values in the figure can be obtained from NACA charts such as those in Fig. 14 (for the example, the wake skew angle is about 82°) to obtain the value of v/v_0, and from Fig. 16 to obtain the value of v_0/v_h for the given operating condition. At this flight condition (advance ratio = 0.167), the inflow distribution is nonlinear, varying from a slight upwash at the leading edge of the rotor to a strong downwash at the trailing edge. In Ref. 11, a linear fit to the test data yields the value of $K_c = 1.43$, which is significantly higher than that calculated from Coleman et al. ($K_c = \tan(\chi/2)=0.87$) as shown in Table 4. For purposes of comparison, three other first-harmonic inflow models listed in Table 2 are included in the table for all three flight conditions tested.

It is evident from the table that the Blake/White model and the Pitt/Peters model better match the linear fit to the test data than the other two models do. It is also interesting to note that the mean induced velocity (or induced velocity at the rotor disc center) of the linear fit to the test data is considerably smaller than that calculated from the momentum theory for all three test conditions. Fig. 32 shows an example of a test condition similar to that shown in Fig. 31. Three additional first-harmonic inflow models, i.e., Blake, Pitt, and Howlett, are included in the original figure in Ref. 11, in which some results from Mangler and Square [12] are also shown.

Table 4. Comparison of Several First-Harmonic Inflow Models with Brotherhood-Steward [11] Flight Data

Parameter	Test conditions		
	1	2	3
Advance ratio	0.138	0.167	0.188
Estimated wake-skew angle, deg	82.8	82.1	84.9
	v_0/v_h		
Momentum	0.34	0.29	0.26
Linear fit to data [11]	0.25	0.26	0.20
	K_c		
Data fit	1.54	1.43	1.94
Coleman	0.88	0.87	0.91
Pitt	1.30	1.28	1.35
Howlett	0.98	0.98	0.99
Blake	1.40	1.40	1.41

In 1976, Landgrebe and Egolf [75,76] extensively correlated their wake analysis (which is generally known as UTRC rotorcraft wake analysis) with induced-velocity test data obtained from 1954 to 1974 from 10 different sources. The analysis included a host of options ranging from the classical skewed helical wake model to a free-wake method, which provides the capability for the calculation of both time-averaged and instantaneous induced velocities at and near a rotor, as described in detail in Refs. 19 and 77. The results of the correlation study indicated that the prediction from the free-wake method was generally in good agreement with the test data, although the accuracy deteriorated near a wake boundary or in the vicinity of the rotor blade, mainly because of the use of lifting line (instead of lifting surface) theory in the analysis. The result of Landgrebe and Egolf's correlation of their wake analysis data with a set of laser velocimeter data obtained by Biggers and Orloff [78] in a wind tunnel at the NASA Ames Research Center is shown in Fig. 33. The test condition was an advance ratio of 0.18 with a TPP angle of attack of –6.6°. The calculated and the measured radial distributions of the vertical velocity component at 90° azimuth position (i.e., advancing side) are shown at four vertical positions beneath the rotor plane for the time-averaged and instantaneous values, respectively, in (a) and (b). The calculated values included those both with and without wake distortion (the wake-distortion version corresponded to the use of their free-wake method). As a result of the passage of the tip vortices, the flow is upward outside the wake and downward inside the wake. The free-wake method tends to better predict the tip vortex position, thereby improving the correlation with the data. However, as can be seen in these figures, the calculated values become significantly degraded as the vortex position approaches the rotor plane.

In 1988, Hoad et al. [2] did extensive correlations between several state-of-the-art analytical rotor wake methods and inflow measurements collected from a wind tunnel at NASA Langley Research Center using a laser velocimeter [1]. The laser data were obtained at various azimuthal and radial positions slightly above the rotor disc plane (z/R = 0.0885) at advance ratios of 0.15, 0.23, and 0.30. The thrust coefficient was 0.0064, and the TPP angle of attack was small, ranging from –3° to –4°. The analytical methods examined included three options (classical skewed-helix wake module, free-wake module, and generalized-wake module) of the UTRC rotorcraft wake analysis [76,79] discussed earlier, the CAMRAD [27] with the Scully free wake [28], and the Beddoes method [80], which utilized a prescribed wake geometry. The results show that, in general, the calculated values, even those calculated from the free-wake methods, do not agree very well with the measured data. The large upwash region in the leading-edge part of the disc, apparent in the measured data, is not reproduced by the calculations. Neither is the largest downwash on the advancing side of the rear portion of the disc matched by the calculated values.

It is of interest to see how well the simple first harmonic inflow models listed in Table 2 perform compared to those sophisticated computer codes just discussed. The four inflow models shown in Fig. 16 were used to calculate the induced velocities at the rotor disc, without corrections for the small vertical position difference, z/R = 0.0885. The results were compared with the measured data for the fore-and-aft radial distributions at the three advance ratios shown in Fig. 34. It is seen that the mean inflow ratio calculated from the momentum theory is considerably larger than the measured values as the advance ratio increases. This trend was also noted previously in the discussion of correlations with the flight data of

Brotherhood and Steward. Failure to consider the wake roll-up and the presence of the induced velocity component parallel to the rotor disc plane might account for the discrepancy. The slope, however, matches the trend of the data fairly well, particularly with the Pitt and Blake models. Correlations for other azimuthal positions show a similar trend, as shown in Fig. 35 for $\mu = 0.15$. To compare more quantitatively the merits or flaws of the first harmonic inflow models, the radial distribution of the inflow angle errors from each of the four models was calculated at various azimuthal positions for all three advance ratios tested. The results show that the first harmonic inflow models compare favorably with those calculated from the free-wake and prescribed-wake methods evaluated by Hoad et al. [2]. Fig. 36 shows an example of such a comparison at the advance ratio of 0.15. At the zero azimuthal position, $\psi = 0$, the first harmonic inflow models produce larger inflow errors in the inboard portion than most of the prescribed- and free-wake codes do; however, in the outboard portion ($r/R > 0.5$), which is more important than the inboard region because of the higher dynamic pressure, all four simple inflow models perform better than the five wake codes do. Similar trends are seen for other azimuthal positions. Overall, the Pitt inflow model seems to perform slightly better than the other three first-harmonic inflow models at the advance ratio of 0.15. However, at the higher advance ratios of 0.23 and 0.30, there seems to be no clearly discernable advantage of one model over the other, as shown in Figs. 37 and 38. From these figures, it can also be seen that, overall, all the simple first-harmonic inflow models perform as well (or as poorly) as the five state-of-the-art prescribed- and free-wake codes do.

Before this section is concluded, a vortex theory using a flat-wake concept that is suitable for higher forward flight should be discussed. The flat-wake theory [22] is based on the assumption that the free vortices leaving the rotor blades form a continuous vortex sheet which is swept back with the free stream without a downward motion. For simplicity in carrying out the integration involved in calculating the induced velocities using the Biot-Savart law, circulation is assumed to be independent of the azimuthal position. The detailed mathematical treatment is described in Refs. 22 and 23. In these references, it is suggested that the theory is generally valid for $\mu > 1.62\sqrt{C_T}$, which corresponds to the wake skew angle, calculated from the momentum theory, of above 80° at $\alpha = 0$. Good results were reported recently by Zhao and Curtiss [33] using the flat-wake theory to treat the influences of the rotor wake on the tail rotor and the tail surfaces. M. D. Takahashi of Ames Research Center recently developed a software module based on Refs. 22 and 33 for rapid calculation of induced velocities at and near the rotor in high-speed forward flight. Good correlation of the calculated values with test data available in Ref. 22 was obtained, as shown in Fig. 39. The data were measured on a plane 10% of the disk radius beneath the rotor disk, at the flight conditions of $C_T = 0.006$ and $\alpha = 0$. Correlation was also performed with the wind tunnel data of Ref. 1. Figure 40 shows the calculated induced inflow ratios at three values of the advance ratios, $\mu = 0.15$, 0.23, and 0.30, all at $\alpha = 0$, $C_T = 0.0064$, and $z/R = 0.0885$ (above the rotor disk). For the purpose of comparison with the data in Figs. 36-38, the inflow angle errors at these data points were also calculated. Figure 41 shows an example of the results at two azimuth positions, $\psi = 0°$ and 180°. It is seen that the correlation of the flat-wake method improves near the trailing edge of the rotor as the advance ratio increases; however, the correlation deteriorates somewhat in the midsection of the rotor. Overall, the results from the flat-wake method compare favorably with the free-wake methods.

3.2 Static Effect Resulting from Aerodynamic Moments

Since, in a steady pitching or rolling motion, the rotor can exert a first-harmonic aerodynamic moment on the airstream, it is reasonable to assume that there would be a first-harmonic inflow distribution. Momentum theory can be applied [32] to determine the gain matrix of the harmonic inflow components in hover. Curtiss [81] has shown that for linear radial distribution of the inflow components in the form of Eq. (7), the inflow components v_c and v_s are related to aerodynamic pitching and rolling moment coefficients by a gain matrix,

$$\begin{Bmatrix} v_s \\ v_c \end{Bmatrix} = -\frac{1}{v_0}\begin{bmatrix} K & 0 \\ 0 & K \end{bmatrix}\begin{Bmatrix} C_l \\ C_m \end{Bmatrix} \tag{12}$$

where the value of K depends on the wake model used. For a "rigid wake model," which assumes that the mass flow used in applying the momentum theory considers only v_0, the value of K is 2. For a "nonrigid wake model," which considers the total inflow, $v = v_0 + v_c \cos\psi + v_s \sin\psi$, in calculating the mass flow when applying the momentum theory, the value of K i s 1. Note that the rigid wake model corresponds to that used in Ref. 40 and the latter to Ref. 42. Gaonkar and Peters [82] provide an extensive review of the development of the gain matrix from a historical perspective, and discuss the implications of the two wake assumptions. Perhaps more experimental data are needed to resolve the controversy resulting from the two different assumptions.

Extension of the gain matrix from hover to forward flight using momentum theory proves to be more difficult and less satisfactory. The gain matrix, developed by Pitt and Peters [44] using unsteady actuator theory, has been correlated extensively and compared favorably [83] with the results using a prescribed wake method contained in the UTRC Rotorcraft Wake Analysis discussed earlier. The gain matrix, L, was further extended by Peters [46] for total, rather than perturbed, values of the thrust coefficient. Expressed in terms of wake-skew angle, it can be shown to be

$$\begin{Bmatrix} v_0 \\ v_s \\ v_c \end{Bmatrix} = [L]\begin{Bmatrix} C_T \\ C_l \\ C_m \end{Bmatrix} \tag{13a}$$

$$L = \begin{bmatrix} \frac{1}{2v_T} & 0 & \frac{15\pi}{64v_m}\tan\frac{\chi}{2} \\ 0 & -\frac{4}{v_m(1+\cos\chi)} & 0 \\ \frac{15\pi}{64v_T}\tan\frac{\chi}{2} & 0 & -\frac{4\cos\chi}{v_m(1+\cos\chi)} \end{bmatrix} \tag{13b}$$

where $v_T = (\mu^2 + \lambda^2)^{1/2}$, and the mass-flow parameter, v_m, is given by

$$v_m = \frac{\mu^2 + \lambda(\lambda + v_0)}{v_T} \tag{14}$$

Note from Eq. (13) that the Glauert gradient term, which represents the ratio of the v_0 to v_c due to thrust, is $(15\pi/64)\tan(\chi/2)$, which was discussed earlier. For hover and for high-speed flight (more precisely, for wake skew angle = 90°), the gain matrix in Eq. (13) reduces to Eqs. (15) and (16), respectively:

$$L_{hover} = \frac{1}{v_0}\begin{bmatrix} \frac{1}{2} & 0 & 0 \\ 0 & -1 & 0 \\ 0 & 0 & -1 \end{bmatrix} \tag{15}$$

$$L_{cruise} = \frac{1}{\mu}\begin{bmatrix} \frac{64}{75\pi} & 0 & -\frac{1}{12} \\ 0 & \frac{64}{45\pi} & 0 \\ \frac{2}{5} & 0 & 0 \end{bmatrix} \tag{16}$$

Note that L_{22} and L_{33} elements in (15) are identical to those derived from the momentum theory using the nonrigid wake assumption discussed earlier. The value of L_{11} is obtained by using the total values of C_T and v_0. When the perturbation values of C_T and v_0 are used as derived in the original Pitt/Peters dynamic inflow model [44], the value of L_{11} is only one-half that shown in Eq. (15) (i.e., $L_{11} = 1/(4v_0)$. Notice also from Eq. (13) that while the sine component of the induced velocity is uncoupled from other components, the steady and cosine components are, in general, closely coupled, and they are functions of both the thrust coefficient and the pitching-moment coefficient. When adopting an inflow model such as those shown in Eqs. (7) and (13) for flight-dynamic analysis, care should be taken that the proper coordinate system is used. The inflow components, and the aerodynamic force (thrust)

and moments (pitching and rolling), are referred to in the wind axis system; therefore, proper coordinate transformations are generally required for applications to flight dynamics.

4. INFLOW MODELS—DYNAMICS

We now turn to the dynamic aspect of the induced velocity. In most of the preceding section (except in the discussion of free-wake methods) it was tacitly assumed that the induced velocity builds up instantaneously, in response to changes in disc-loading or aerodynamic moments, to its new inflow state. Since a large mass of air must be accelerated to reach the new inflow state, there will be dynamic lag associated with the buildup of induced velocity. For a finite-state characterization of the induced velocity, such as the Pitt/Peters inflow model (a three-state model for the induced velocity at the rotor disc), there will be time constants associated with the buildup of the three inflow components. For a nonfinite-state characterization of the induced velocity, such as a free-wake model, the evolution of the induced velocities at and near the lifting rotor is in consonance with the development of the vortex wake geometry and the blade loading. In this case, however, there are no explicitly defined states or time constants associated with the dynamic process. It is conceivable that a finite-state dynamic model may be used to fit the data generated for the specific area of interest (such as at the rotor disc) from the original free-wake model, but the procedure would be tedious.

For simulation of rotorcraft flight dynamics in a higher frequency range than that of the rigid-body modes, dynamic interactions between the inflow dynamics and the blade motion must be considered. Recent studies [32-34,50] have indicated that, because the frequencies of the inflow dynamic modes are of the same order of magnitude as those of the rotor blade flapping and lead-lag modes, strong dynamic coupling can be present, influencing the stability of the rotorcraft. For nonlinear simulation, particularly in a nonreal-time environment, nonfinite-state, free-wake methods may find wide application in the future because of the rapidly expanding computational power at reduced cost. However, finite-state inflow models such as those of Pitt/Peters [44] and Peters/He [84] are better suited for linear analysis or for real-time simulation of rotorcraft flight dynamics. For this reason, the discussion that follows is focused on the finite-state dynamic inflow models.

According to the updated version of the Pitt/Peters dynamic inflow theory for a three-state model [47,82] suitable for flight-dynamic applications, the apparent mass matrix, M, in the dynamic inflow equation,

$$M\begin{Bmatrix} v_0 \\ v_s \\ v_c \end{Bmatrix}^{*} + L^{-1}\begin{Bmatrix} v_0 \\ v_s \\ v_c \end{Bmatrix} = \begin{Bmatrix} C_T \\ C_l \\ C_m \end{Bmatrix} \tag{17}$$

is given by

$$M = \begin{bmatrix} \frac{8}{3\pi} & 0 & 0 \\ 0 & -\frac{16}{45\pi} & 0 \\ 0 & 0 & -\frac{16}{45\pi} \end{bmatrix} \tag{18}$$

in which the M_{11} element was suggested to be $128/75\pi$ for rotors with twisted blades [47]. (The value of M_{11} in Eq. (18) and the suggested value for a twisted blade correspond respectively to "uncorrected" and "corrected" values stated in the original Pitt/Peters model [44]). Recent studies [45,85] have found, however, that the value of $M_{11} = 8/3\pi$, which is identical to that originally proposed by Carpenter and Fridovich [13], correlates better with the flight-test data, even though the rotor blades are twisted.

The matrix of time constants associated with the inflow dynamics is obtained by multiplying both sides of Eq. (17) by the static gain matrix, L, to yield

$$[\tau]\begin{Bmatrix} v_0 \\ v_s \\ v_c \end{Bmatrix}^* + \begin{Bmatrix} v_0 \\ v_s \\ v_c \end{Bmatrix} = [L]\begin{Bmatrix} C_T \\ C_l \\ C_m \end{Bmatrix} \tag{19}$$

where

$$[\tau] = LM = \begin{bmatrix} \frac{1}{v_T}\frac{4}{3\pi} & 0 & -\frac{1}{12v_m}\tan\frac{\chi}{2} \\ 0 & \frac{64}{45\pi v_m(1+\cos\chi)} & 0 \\ \frac{5}{8v_T}\tan\frac{\chi}{2} & 0 & \frac{64\cos\chi}{45\pi v_m(1+\cos\chi)} \end{bmatrix} \tag{20}$$

Values of the time constant matrix in hover and in edgewise flight (i.e., $\chi = 90°$) are therefore given by

$$[\tau]_{\text{hover}} = \frac{1}{v_0}\begin{bmatrix} \frac{4}{3\pi} & 0 & 0 \\ 0 & \frac{16}{45\pi} & 0 \\ 0 & 0 & \frac{16}{45\pi} \end{bmatrix} \tag{21}$$

$$[\tau]_{\text{cruise}} = \frac{1}{\mu}\begin{bmatrix} \frac{4}{3\pi} & 0 & -\frac{1}{12} \\ 0 & \frac{64}{45\pi} & 0 \\ \frac{5}{8} & 0 & 0 \end{bmatrix} \tag{22}$$

It is of interest that in hover the time-constant matrix is diagonal, as is the static gain matrix, L, discussed in the preceding section. Equation (21) is identical to that derived based on the momentum theory with the nonrigid-wake assumption [32]. If the rigid-wake assumption is used, the time constants associated with the harmonic inflow variations resulting from changes in moments (i.e., τ_{22} and τ_{33}) are twice as large as those shown in Eq. (21) because, as explained earlier, the static gains are. Correlations with wind tunnel data obtained from a hingeless rotor model in hover [82,86,87] produced mixed results using the two different wake assumptions. More work is needed to resolve this controversial "factor of two" problem. For detailed discussions of the historical development of the dynamic inflow models, the reader is referred to the excellent review paper of Gaonkar and Peters [82].

5. SUMMARY

A brief survey of nonuniform inflow models for the calculation of induced velocities at and near a lifting rotor has been conducted from the perspective of flight dynamics and control applications. The survey covers hover and low-speed and high-speed flight, both in and out of ground effect. A primary emphasis has been placed on the evaluation of various simple first-harmonic inflow models developed over the years, in comparison with more sophisticated methods developed for use in performance and structure disciplines. Both static and dynamic aspects of the inflow were reviewed; however, only the static aspect is considered in the comparative evaluation using available old and new test data. Results from this limited correlation effort are somewhat surprising. At the rotor out of ground effect, all the first-harmonic inflow models predict the induced velocity as well (or as poorly) as the free-wake methods reviewed when compared to a set of new data at advance ratios of 0.15, 0.23, and 0.30. The results of correlation with several sets of test data indicate that the Pitt/Peters first-harmonic inflow model works well overall. For inflow near the rotor or in ground effect, it is suggested that charts similar to those of Heyson/Katzoff and Castles/De Leeuw of NACA should be produced using modern free-wake methods for use in flight-dynamic analyses and

simulations. Finally, it is suggested that additional experiments be conducted to resolve issues concerning the influence of mass flow assumptions on aerodynamic moments and time constants associated with inflow dynamics.

REFERENCES

1. Elliott, J. W. and Althoff, S. L., Inflow Measurement Made with a Laser Velocimeter on a Helicopter Model in Forward Flight, NASA TM 100541-100543, April 1988.

2. Hoad, D. R., Althoff, S. L., and Elliott, J. W., Rotor Inflow Variability with Advance Ratio, Ann. Forum AHS, June 1988.

3. Glauert, H., A General Theory of the Autogyro, R&M No. 1111, British A.R.C., 1926.

4. Wheatley, J. B., An Aerodynamic Analysis of the Autogiro Rotor with a Comparison Between Calculated and Experimental Results, NACA Report No. 487, 1934.

5. Seibel, C., Periodic Aerodynamic Forces on Rotors in Forward Flight, J. Aero. Sci., Vol. 11, No. 4, pp. 339-342, Oct. 1944.

6. Coleman, R. P., Feingold, A. M., and Stempin, C. W., Evaluation of the Induced-Velocity Field of an Idealized Helicopter Rotor, NACA ARR L5E10, 1945.

7. Drees, J. M. Jr., A Theory of Airflow Through Rotors and its Application to Some Helicopter Problems, J. Helicopter Assoc. Great Britain, Vol. 3, No. 2, July-Sept. 1949.

8. Brotherhood, P., An Investigation in Flight of Induced Velocity Distribution Under a Helicopter Rotor When Hovering, Br. ARC RAE Report No. Aero.2212, June 1947.

9. Gessow, A. and Myers, G. C. Jr., Aerodynamics of the Helicopter, Frederick Ungar Pub. Co., New York, 1952.

10. Gessow, A., Review of Information on Induced Flow of a Lifting Rotor, NACA TN 3238, 1954.

11. Brotherhood, P. and Steward, W., An Experimental Investigation of the Flow Through a Helicopter Rotor in Forward Flight, R&M No. 2734, Sept. 1949.

12. Mangler, K. W. and Square, H. B., The Induced Velocity Field of a Rotor, R&M No. 2642, May 1950.

13. Carpenter, P. J. and Fridovich, B., Effect of a Rapid-Pitch Response of the Thrust and Induced-Velocity Response of a Full-Scale Helicopter Rotor, NACA TN 3044, 1953.

14. Castles, W. Jr. and De Leeuw, J. H., The Normal Component of the Induced Velocity in the Vicinity of a Lifting Rotor and Some Examples of Its Application, NACA Rept. 1184, 1954.

15. Heyson, H. H. and Katzoff, S., Induced Velocities Near a Lifting Rotor with Nonuniform Disk Loading, NACA Rept. 1319, 1957.

16. Jewel, J. W. Jr. and Heyson, H. H., Charts of the Induced Velocities Near a Lifting Rotor, NASA MEMO 4-15-59L, May 1959.

17. Piziali, R. A. and Du Waldt, F. A., A Method for Computing Rotary Wing Airload Distributions in Forward flight, U.S.Army TRECOM Rept. No. TCREC TR 62-44, Nov. 1962.

18. Davenport, F. J., A Method for Computation of the Induced Velocity Field of a Rotor in Forward Flight Suitable for Application to Tandem Rotor Configurations, J. AHS, Vol. 9, No. 3, July 1964.

19. Landgrebe, A. J., An Analytical Method for predicting Rotor Wake Geometry, J. AHS, Vol. 14, No. 4, Oct. 1969.

20. Sadler, S. G., Development and Application of a Method for Predicting Free Wake Positions and Resulting Rotor Blade Air Loads, Vol. 1—Model and Results, NASA CR-1911, 1971.

21. Heyson, H. H., A Brief Survey of Rotary Wing Induced Velocity Theory, NASA TM 78741, June 1978.

22. Baskin, V. E., Vil'dgrube, L. S., Vozhdayev, Ye. S., and Maykapar, G. I., Theory of the Lifting Airscrew, NASA TTF-823, Feb. 1976.

23. Stewpniewski, W. Z. and Keys, C. N., Rotary-Wing Aerodynamics, Vol. I—Basic Theories of Rotor Aerodynamics (with Application to Helicopters), NASA CR-3082, Jan. 1979.

24. Harris, F. D., Articulated Rotor Blade Flapping Motion at Low Advance Ratio, J. AHS, Vol. 17, No. 4, Jan. 1972.

25. Ruddell, A. J., Advancing Blade Concept (ABC™) Development, Ann. Forum AHS, May 1976.

26. Johnson, W., Comparison of Calculated and Measured Helicopter Rotor Lateral Flapping Angles, J. AHS, Vol. 26, No. 2, April 1981.

27. Johnson, W., A Comprehensive Analytical Model of Rotorcraft Aerodynamics and Dynamics Part 1: Analysis and Development, NASA TM 81182, June 1980.

28. Scully, M. P., Computation of Helicopter Rotor Wake Geometry and its Influence on Rotor Harmonic Airloads, Massachusetts Institute of Technology, ASRL TR 178-1, March 1975.

29. Miller, R. H., Ellis, S. C., and Dadone, L., The Effects of Wake Migration During Roll-up on Blade Air Loads, Vertica, Vol. 13, No. 1, pp. 1-15, 1989.

30. Bliss, D. B. and Miller, W. O., Efficient Free Wake Calculation Using Analytical/ Numerical Matching and Far-field Linearization, Ann. Forum AHS, May 1989.

31. Howlett, J. J., UH-60A Black Hawk Engineering Simulation Program: Vol. I— Mathematical Model, NASA CR-66309, 1981.

32. Curtiss, H. C. Jr., Stability and Control Modelling, 12th European Rotorcraft Forum, Garmisch-Patenkirchen, FRG, Sept. 1986.

33. Zhao, X. and Curtiss, H. C. Jr., A Linearized Model of Helicopter Dynamics Including Correlation with Flight Test, Proc. 2nd Intern. Conf. Rotorcraft Basic Res., Univ. of Maryland, College Park, MD., Feb. 1988.

34. Schrage, D. P., et al., Helicopter Stability and Control Modeling Improvements and Verification on Two Helicopters, 14th European Rotorcraft Forum, Milano, Italy, Sept. 1988.

35. Curtiss, H. C. Jr. and Shupe, N. K., Stability and Control Theory for Hingeless Rotors, Ann. Forum AHS, May 1971.

36. Ormiston, R. A. and Peters, D. A., Hingeless Helicopter Rotor Response with Nonuniform Inflow and Elastic Blade Bending, J. Aircraft,Vol. 9, No. 10, Oct. 1972.

37. Peters, D. A., Hingeless Rotor Frequency Response with Unsteady Inflow, in NASA SP-362, Feb. 1974.

38. Crews, S. T., Hohenemser, K. H., and Ormiston, R. A., An Unsteady Wake Model for a Hingeless Rotor, J. Aircraft, Vol. 10, No. 12, Dec. 1973.

39. Ormiston, R. A., Application of Simplified Inflow Models to Rotorcraft Dynamic Analysis, J. AHS, Vol. 21, No. 3, July 1976.

40. Johnson, W., Influence of Unsteady Aerodynamics on Hingeless Rotor Ground Resonance, J. Aircraft, Vol. 19, No. 8, Aug. 1982.

41. Johnson, W., Helicopter Theory, Princeton Univ. Press, 1980.

42. Banerjee, D., Crews, S. T., Hohenemser, K. H., and Yin, S. K., Identification of State Variables and Dynamic Inflow from Rotor Model dynamic Tests, J. AHS, Vol. 22, No. 2, April 1977.

43. Banerjee, D., Crews, S. T., and Hohenemser, K. H., Parameter Identification Applied to Analytic Hingeless Rotor Modeling, J. AHS, Vol. 24, No. 1, Jan. 1979.

44. Pitt, D. M. and Peters, D. A., Theoretical Prediction of Dynamic Inflow Derivatives, Vertica, Vol. 5, pp. 21-34, 1981.

45. Chen, R. T. N. and Hindson, W. S., Influence of Dynamic Inflow on the Helicopter Vertical Response, Vertica, Vol. 11, No. 1-2, pp. 77-91, 1987.

46. Peters, D. A., The Influence of Steady and Dynamic Inflow on the Stability of Rotor-Body System, Proc. ITR Methodology Workshop, NASA Ames, June 1983.

47. Peters, D. A. and HaQuang, N., Dynamic Inflow for Practical Application, J. AHS, Vol. 33, No. 4, Oct. 1988.

48. Harris, F. D., Rotary Wing Aerodynamics—Historical Perspective and Important Issues, National Specialists' Meeting on Aerodynamics and Aeroacoustics, Fort Worth, TX, Feb. 1987.

49. White, F. and Blake, B. B., Improved Method of Predicting Helicopter Control Response and Gust Sensitivity, Ann. Forum AHS, May 1979.

50. Miller, D. G. and White, F., A Treatment of the Impact of Rotor-Fuselage Coupling on Helicopter Handling Qualities, Ann. Forum AHS, St. Louis, MO, May 1987.

51. Payne, P. R., Helicopter Dynamics and Aerodynamics, Sir Isaac Pitman & Sons, LTD. London, 1959.

52. Meijer Drees, J. and Hendal, W. P., Airflow Patterns in the Neighbourhood of Helicopter Rotors, Aircraft Engineering, Vol. 23, No. 266, April 1951.

53. Bliss, D. B., et al., A New Approach to the Free Wake Problem for Hovering Rotors, Ann. Forum AHS, May 1985.

54. Kocurek, J. D., Berkowitz, L. F., and Harris, F. D., Hover Performance Methodology at Bell Helicopter Textron, Ann. Forum AHS, May 1980.

55. Landgrebe, A. J., The Wake Geometry of a Hovering Helicopter Rotor and Its Influence on Rotor Performance, J. AHS, Vol. 17, No. 4, Oct. 1972.

56. Landgrebe, A. J., An Analytical and Experimental Investigation of Helicopter Rotor Hover Performance and Wake Geometry Characteristics, USAAMRDL TR 71-24, June 1971.

57. Prouty, R. W., Helicopter Performance, Stability and Control, PWS Engineering, Boston, MA, 1986.

58. Knight, M. and Hefner, R. A., Analysis of Ground Effect of the Lifting Airscrew, NACA TN 835, Dec. 1941.

59. Heyson, H. H., Theoretical Study of the Effect of Ground Proximity on the Induced Efficiency of Helicopter Rotors, NASA TMX-71951, May 1977.

60. Schrage, D. A. and Peskar, R. E., Helicopter Vibration Requirements, Ann. Forum AHS, May 1977.

61. Reichert, G., Helicopter Vibration Control—A survey, 6th European Rotorcraft and Power Lift Aircraft Forum, Bristol, England, 1980.

62. Cheeseman, I. C. and Haddow, C., An Experimental Investigation of the Downwash Beneath a Lifting Rotor and Low Advance Ratios, 14th European Rotorcraft Forum, 1988.

63. Chen, R. T. N., Selection of Some Rotor Parameters to Reduce Pitch-Roll Coupling of Helicopter Flight Dynamics, National Specialists' Meeting on Rotor System Design, Philadelphia, PA, 1980.

64. Van Gaasbeek, J. R., et al., Rotorcraft Flight Simulation Computer Program, C-81 with DATAMAP Interface, Vols. I and II, USAAVRADCOM TR-80-D-38A and B, Dec. 1979.

65. Faulkner, A. J. and Buchner, F., Flight Investigations of a Helicopter Low Airspeed Estimation System Based on Measurement of Control Parameters, 6th European Rotorcraft Forum, 1980.

66. Heyson, H. H., Ground Effect for Lifting Rotors in forward Flight, NASA TND-234, May 1960.

67. Cheeseman, I. C. and Bennett, W. E., The Effect of the Ground on a Helicopter Rotor in Forward Flight, British R&M No. 3021, Sept. 1955.

68. Sheridan, P. F. and Wiesner, W., Aerodynamics of Helicopter Flight Near the Ground, Ann. Forum AHS, May 1977.

69. Fradenburgh, E. A., The Helicopter and the Ground Effect Machine, J. AHS, Vol. 5, pp. 24-33, Oct. 1960.

70. Sun, M., A Study of Helicopter Rotor Aerodynamics in Ground Effect at Low Speeds, Ph.D. Thesis, Princeton Univ., Dept. of Mech. Aerospace Eng., June 1983.

71. Sheridan, P. F., et al., Math Modeling for Helicopter Simulation of Low Speed, Low Altitude and Steeply Descending Flight, NASA CR-166385, July 1982.

72. Tischler, M. B., et al., Flight Dynamics Analysis and Simulation of Heavy Lift Airships, Systems Technology, Inc. TR 1151-2-II, Dec. 1982.

73. Curtiss, H. C. Jr., Ground Effect Aerodynamics, Proc. Intern. Conf. Rotorcraft Basic Res., Research Triangle Park, NC, Feb. 19-21, 1985.

74. Curtiss, H. C. Jr., et al., Rotor Aerodynamics in Ground Effect at Low Advance Ratios, J. AHS, Vol. 29, No. 1, Jan. 1984.

75. Landgrebe, A. J. and Egolf, T. A., Prediction of Helicopter Induced Flow Velocities Using the Rotorcraft Wake analysis, Ann. Forum AHS, May 1976.

76. Landgrebe, A. J. and Egolf, T. A., Rotorcraft Wake Analysis for the Prediction of Induced Velocities, USAAMRDL TR-75-45, Jan. 1976.

77. Landgrebe, A. J. and Cheney, M. C. Jr., Rotor Wake—Key to Performance Prediction, AGARD CP-111, Sept. 1972.

78. Biggers, J. C. and Orloff, K. L., Laser Velocimeter Measurements of the Helicopter Rotor-Induced Flow Field, J. AHS, Vol. 20, No. 2, Jan. 1975.

79. Egolf, T. A. and Landgrebe, A. J., Helicopter Rotor Wake Geometry and Its Influence in Forward Flight, Vol. I—Generalized Wake Geometry and Wake Effect on Rotor Airloads and Performance, NASA CR-3726, Oct. 1983.

80. Beddoes, T. S., A Wake Model for High Resolution Airloads, Proc. Int. Conf. Rotorcraft Basic Res., Research Triangle Park, NC, Feb. 1985.

81. Curtiss, H. C. Jr., Dynamic Inflow Effect on Blade Flapping in Hovering Flight, Private communication, 1986.

82. Gaonkar, G. H. and Peters, D. A., Review of Dynamic Inflow Modeling for Rotorcraft Flight Dynamics, Vertica, Vol. 12, No. 3, pp. 213-242, 1988.

83. Pitt, D. M. and Peters, D. A., Rotor Dynamic Inflow Derivatives and Time Constants From Various Inflow Models, 9th European Rotorcraft Forum, Stresa, Italy, Sept. 13-15, 1983.

84. Peters, D. A. and He, C. J., Comparison of Measured Induced Velocities with Results from a Closed-form Finite State Wake Model in Forward Flight, Ann. Forum AHS, May 1989.

85. Houston, S. S. and Tarttelin, P. C., Theoretical and Experimental Correlation of Helicopter Aeromechanics in Hover, Ann. Forum AHS, May 1989.

86. Bousman, W. G., A Comparison of Theory and Experiment for Coupled Rotor-Body Stability of a Hingeless Rotor Model in Hover, ITR Methodology Assessment Workshop, NASA Ames Research Center, June 21-22, 1983.

87. Friedman, P. P. and Venkatesan, C., Influence of Various Unsteady Aerodynamic Models on the Aeromechanical Stability of a Helicopter in Ground Resonance, Second Decennial Specialist's Meeting on Rotor Dynamics, AHS-NASA Ames, Nov. 7-9, 1984.

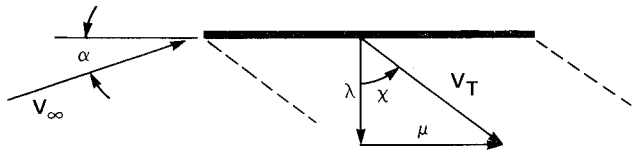

WAKE SKEW ANGLE:

$$\tan \chi = \frac{\mu}{\lambda} \; ; \; \mu = \frac{V_\infty \cos\alpha}{\Omega R}$$

$$\lambda = v_o - \frac{V_\infty \sin\alpha}{\Omega R}$$

Figure 1. Wake skew angle.

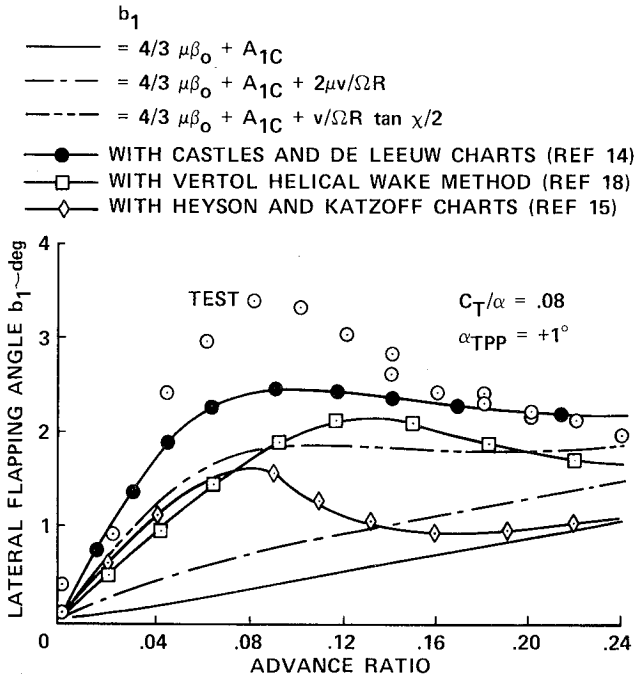

Figure 2. Comparison of calculated lateral flapping angles using several inflow models with test data (from Ref. 24).

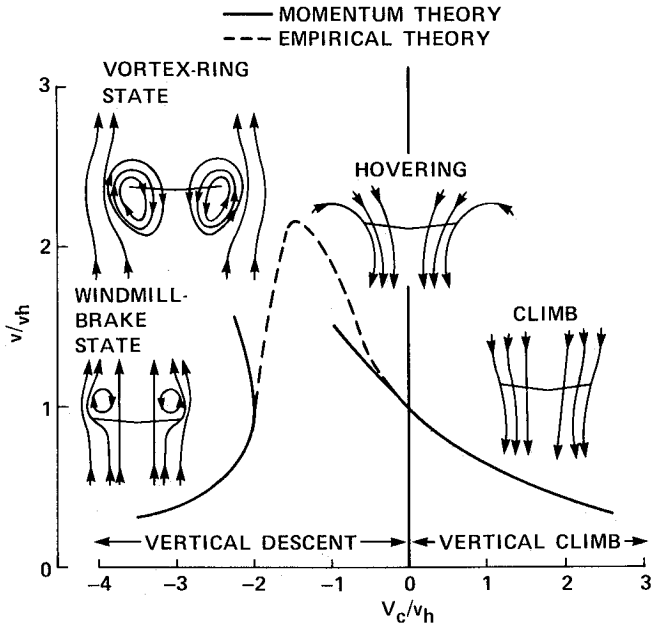

Figure 3. Induced velocity relations in vertical flight (from Ref. 10).

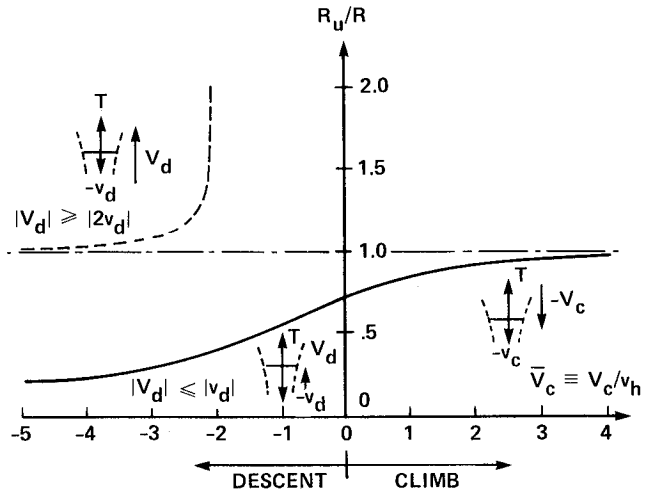

Figure 4. Ratio of fully developed wake radius to that of the actuator disk vs. V_c (from Ref. 23).

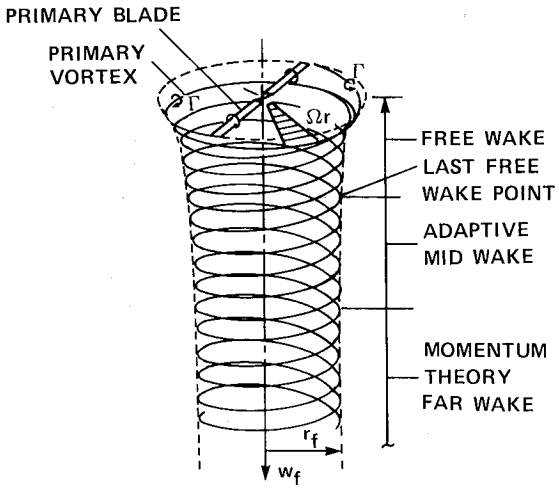

Figure 5. Three-part wake model for the hover analysis (from Ref. 53).

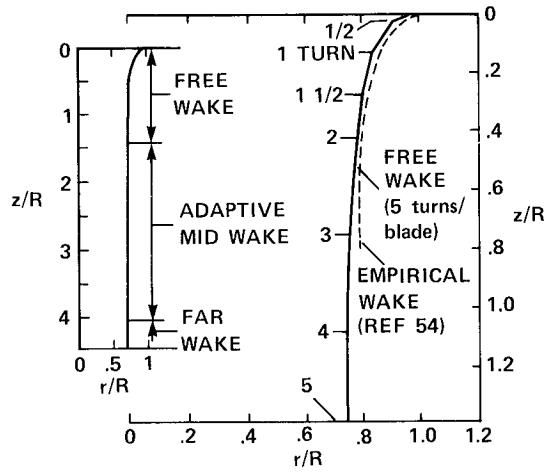

Figure 6. Computed wake envelope for a two-bladed rotor having five turns of free wake per blade with C_T =.0058 (from Ref. 53).

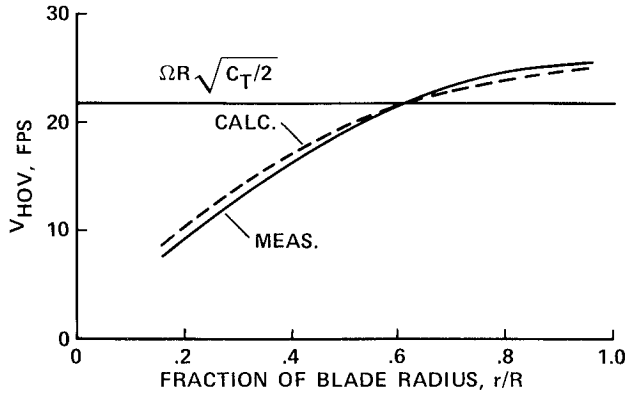

Figure 7. Comparison of calculated uniform and nonuniform inflow with measurements.

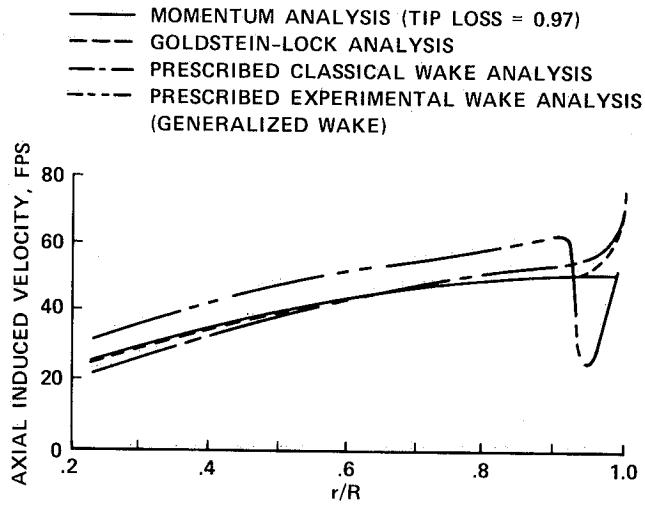

Figure 8. Comparison of induced velocities calculated from momentum theory and three prescribed-wake analyses (from Ref. 56).

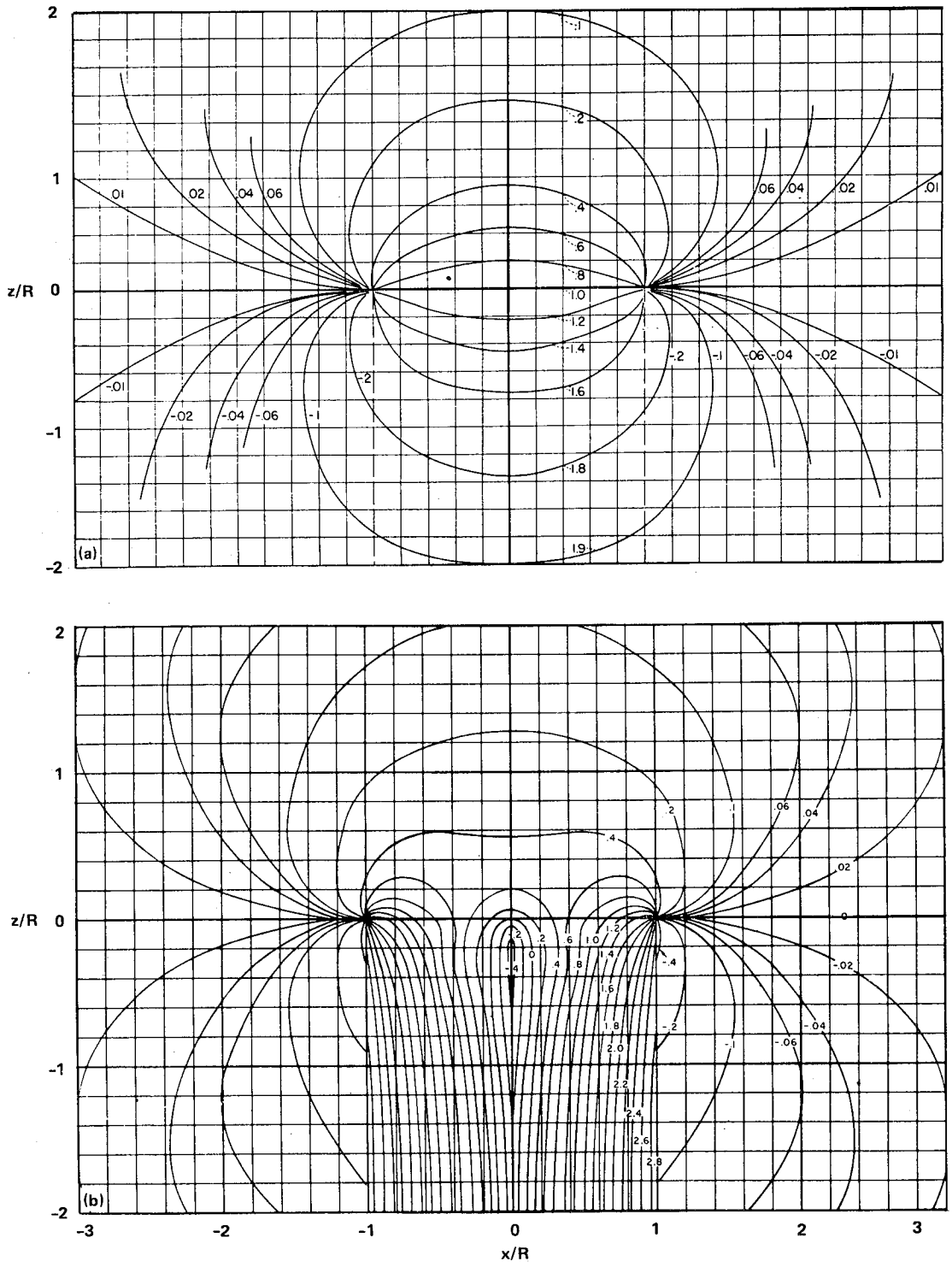

Figure 9. Contours of induced-velocity ratio v/v_0 in the longitudinal plane of the rotor for two different disk loadings at $\chi = 0°$ (from Ref. 16).

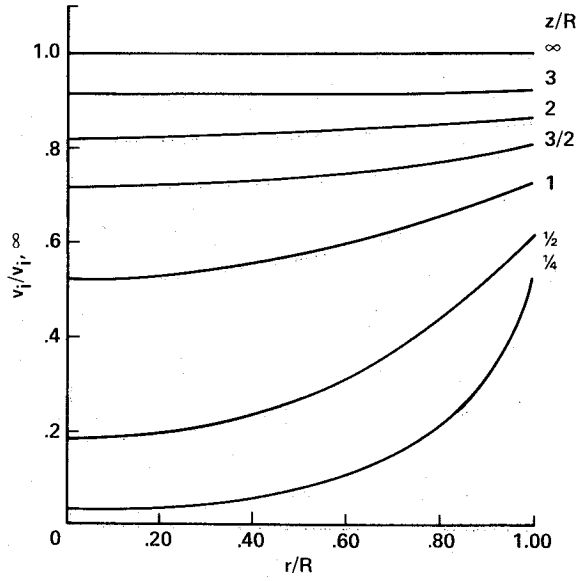

Figure 10. Induced-velocity distribution along rotor blade in ground effect (from Ref. 58).

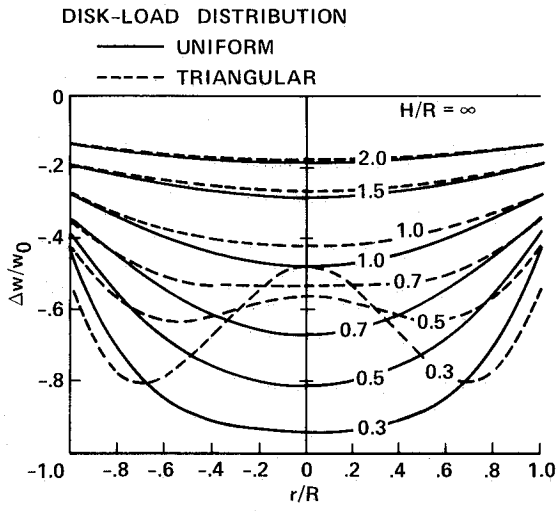

Figure 11. Distribution of ground-induced interference velocities over the longitudinal axis of the rotor in hover (from Ref. 59).

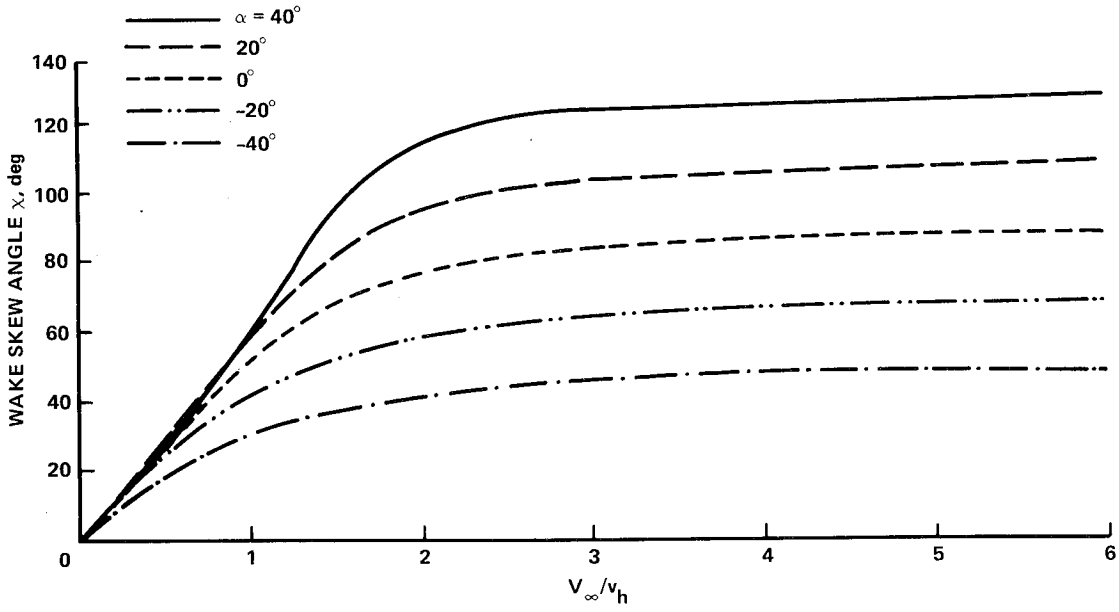

Figure 12. Wake skew angle vs. normalized flight velocity at several values of tip-path plane angle of attack.

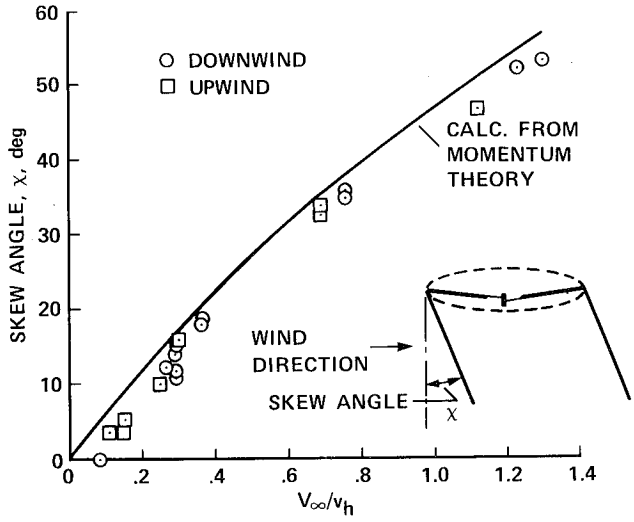

Figure 13. Comparison of calculated and measured wake skew angles at low speeds (from Ref. 10).

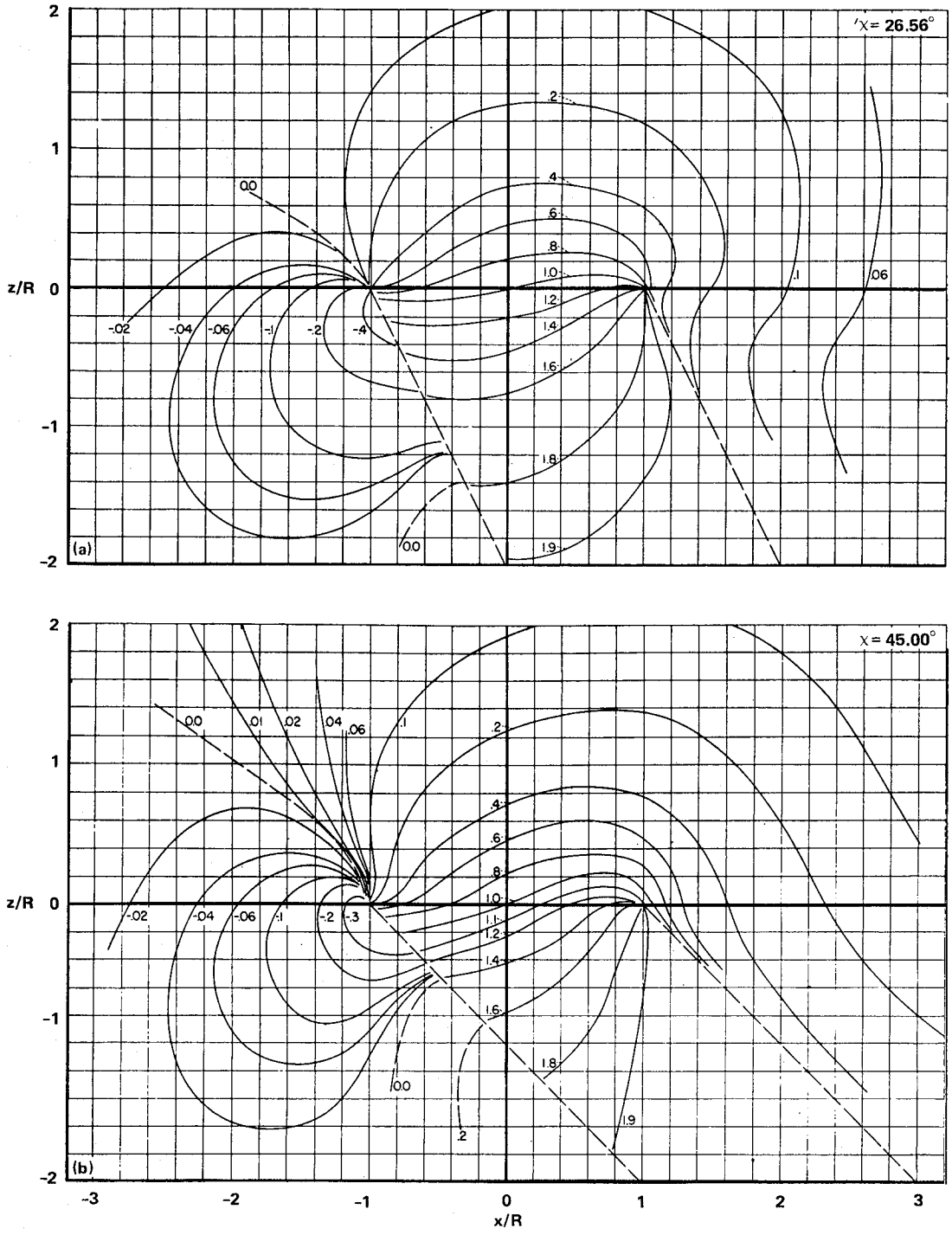

Figure 14. Lines of constant values of isoinduced velocity ratio v/v_0 in longitudinal plane of symmetry for several wake skew angles (from Ref. 16). (a) χ =26.56°. (b) χ = 45°.

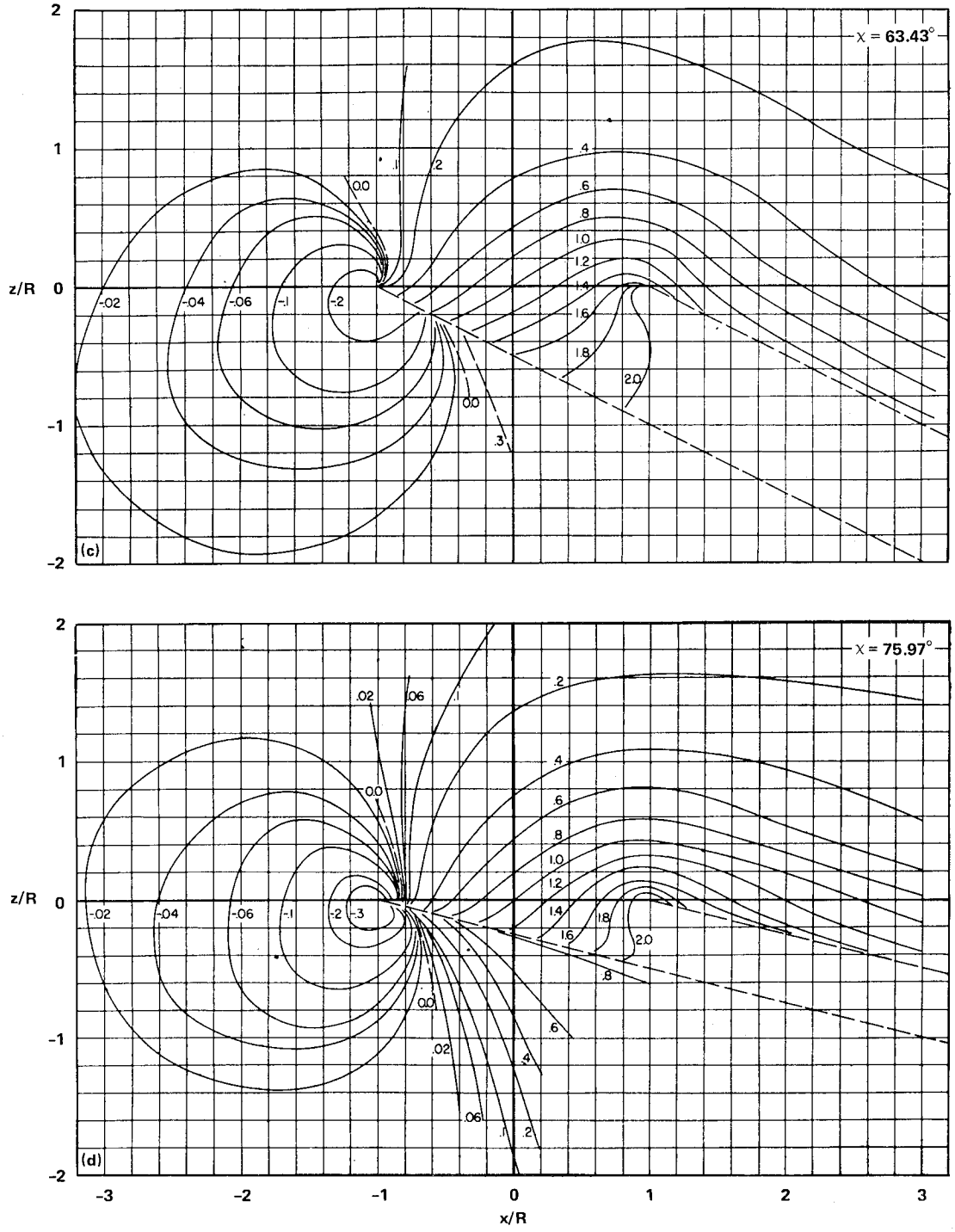

Figure 14. Concluded. (c) $\chi = 63.43°$. (d) $\chi = 75.97°$.

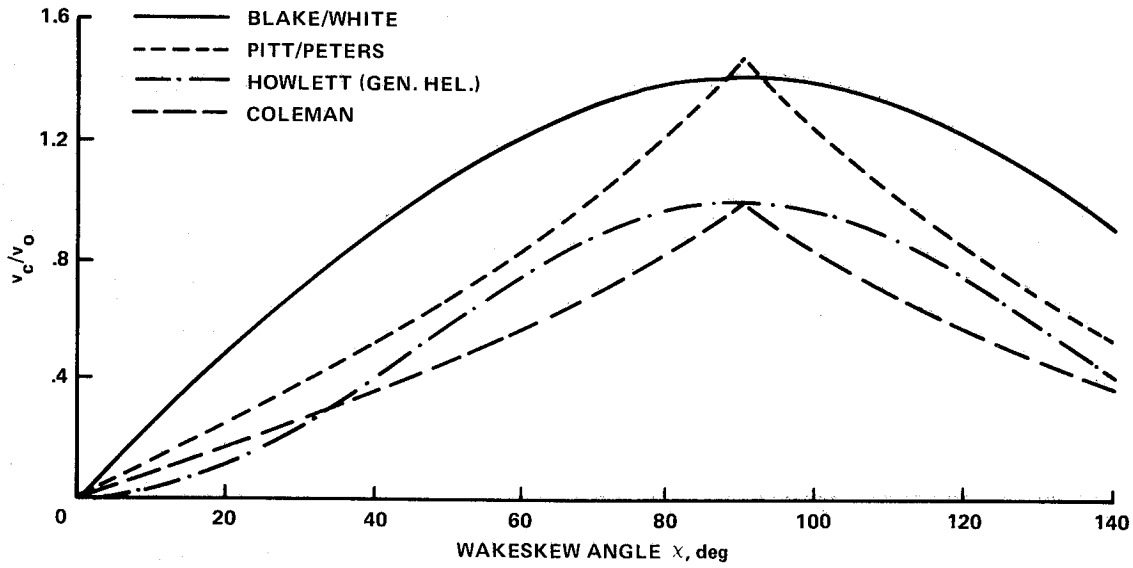

Figure 15. Comparison of v_c/v_0 for several inflow models.

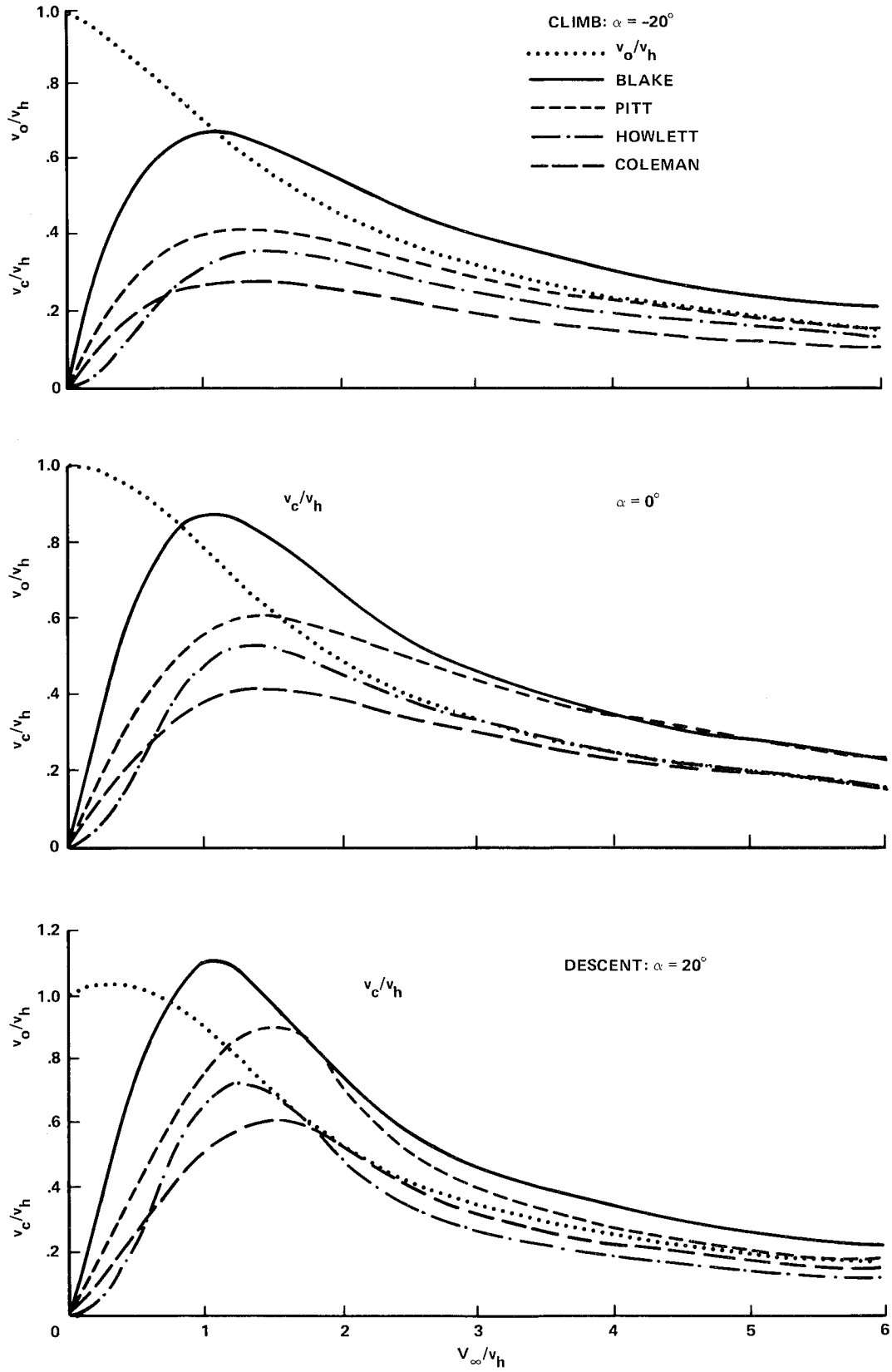

Figure 16. Comparison of v_c/v_h vs. V_∞/v_h for several inflow models at three values of TPP angle of attack.

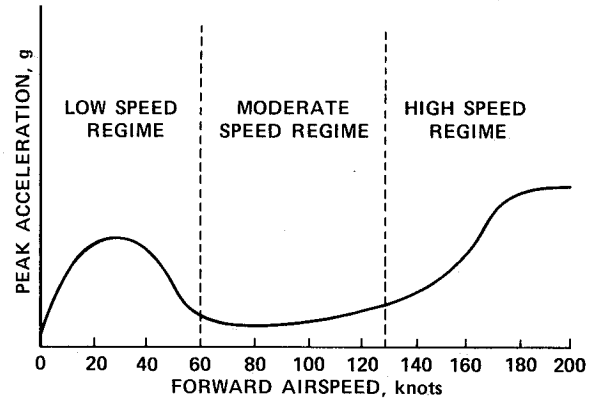

Figure 17. Typical helicopter vibration characteristics with increasing airspeed (from Ref. 60).

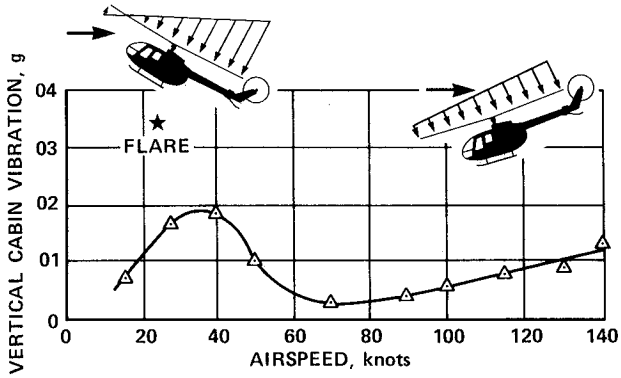

Figure 18. Vibration characteristics for a four-bladed single rotor helicopter (from Ref. 61).

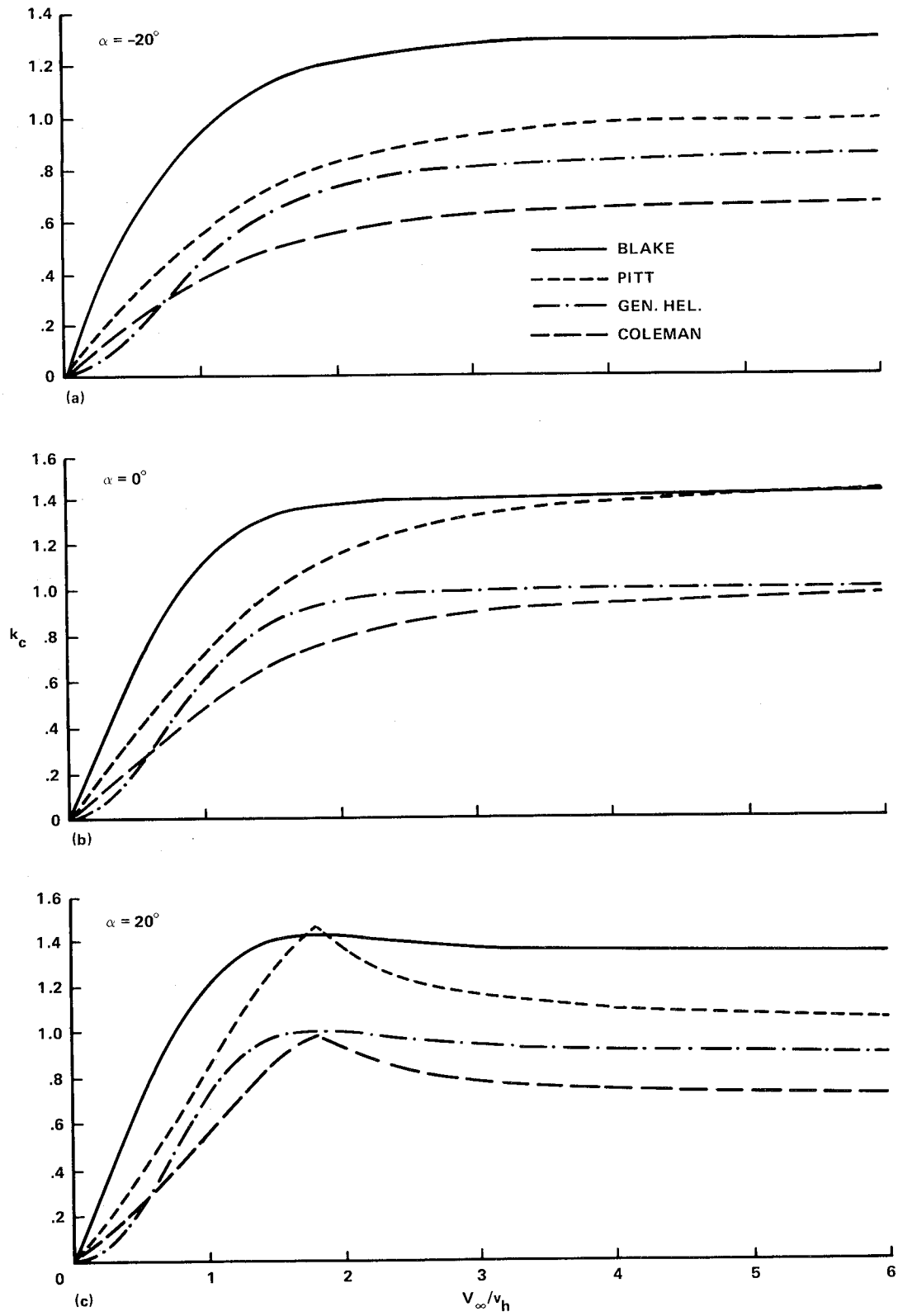

Figure 19. Comparison of K_c values of several inflow models at three values of TPP angle of attack.

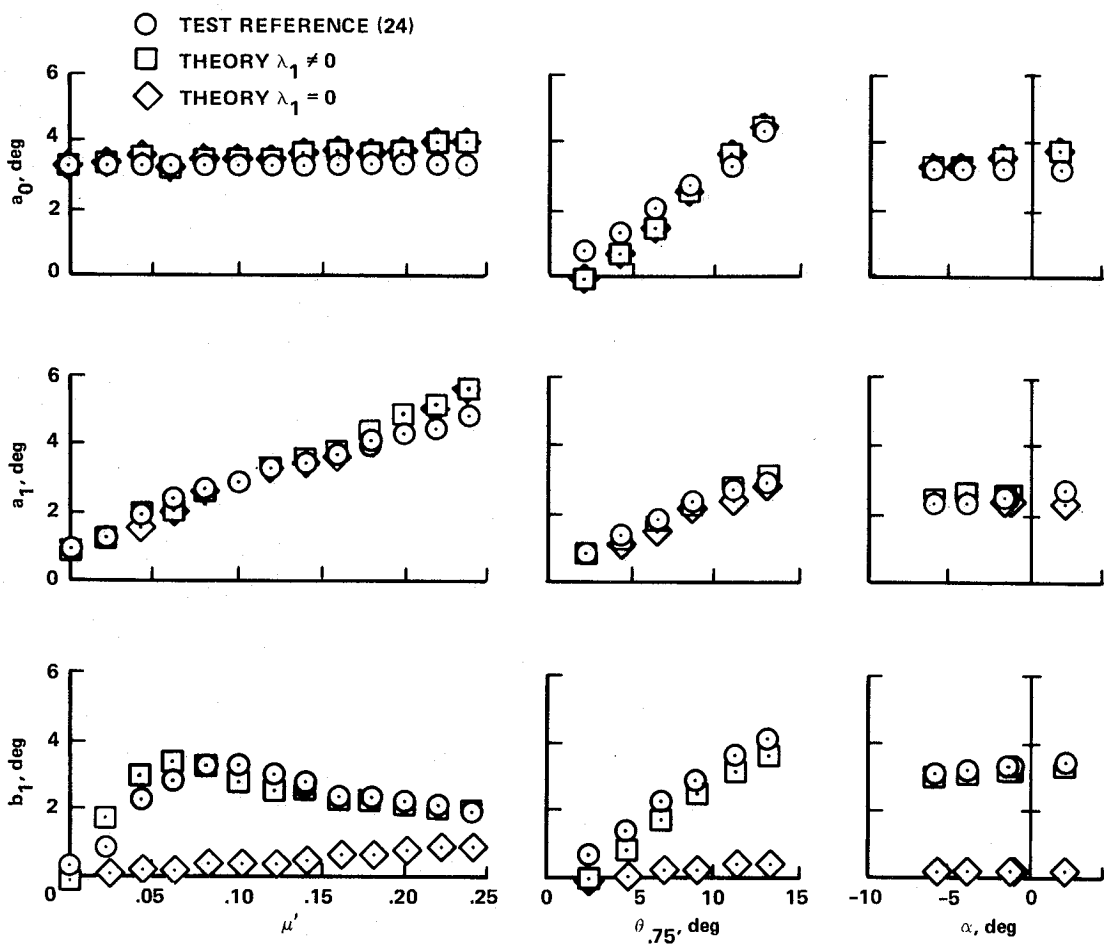

Figure 20. Correlation of calculated flapping angles using the Blake/White inflow model with Harris' test data (from Ref. 63).

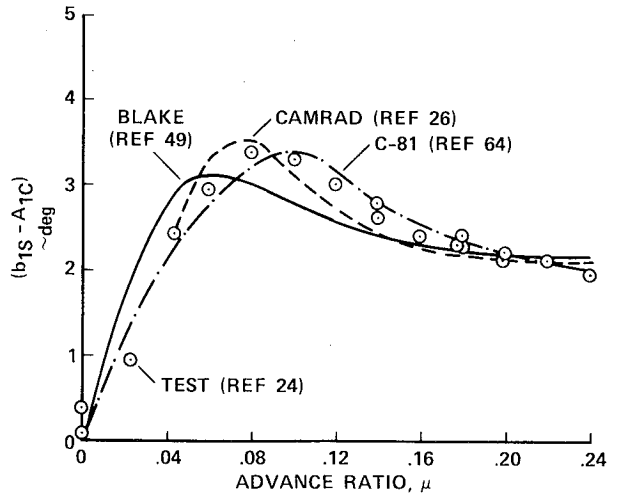

Figure 21. Prediction of lateral flapping is improving (from Ref. 48).

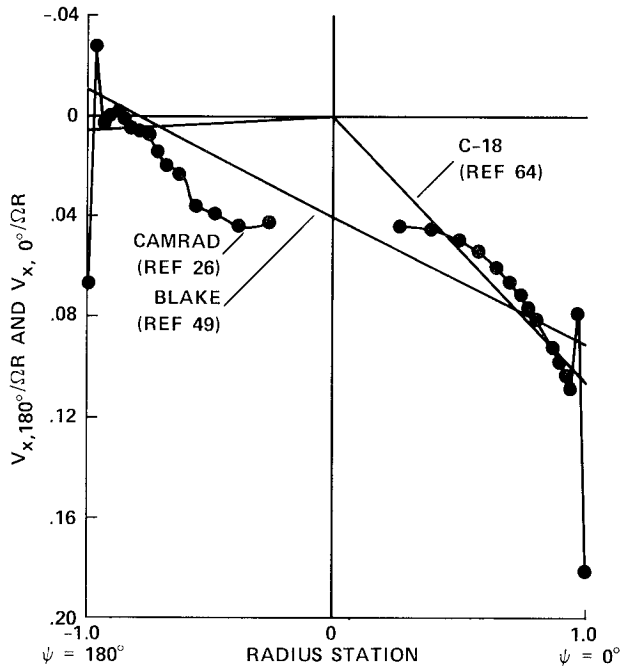

Figure 22. Induced velocity distribution in the plane of symmetry is sort of triangular at $\mu = 0.08$, $\alpha_{TPP} = 1.4°$, $C_T/\sigma = 0.08$ (from Ref. 48).

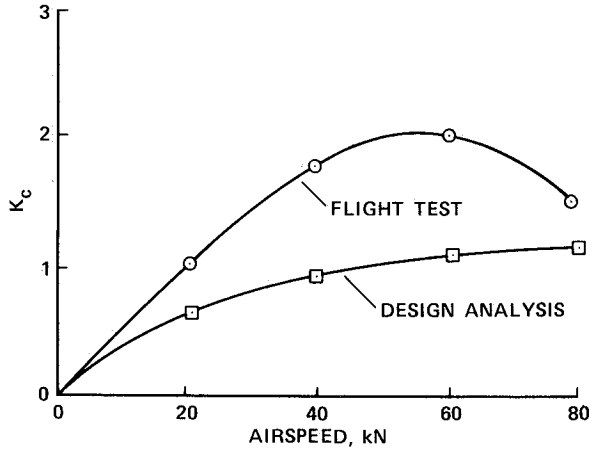

Figure 23. Comparison of K_c values used in the design analysis and determined from flight test (from Ref. 25).

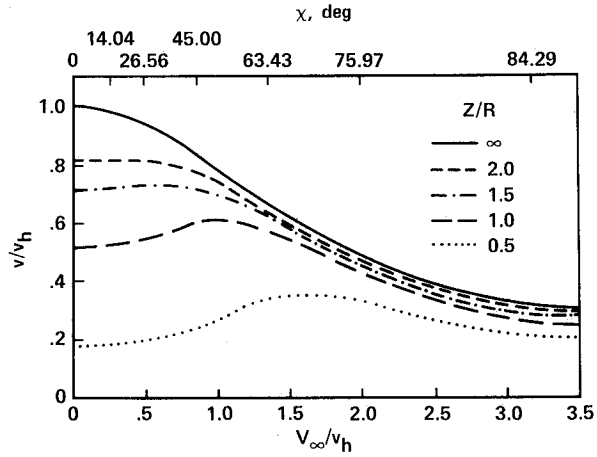

Figure 24. Induced velocity at center of rotor in forward flight near the ground (from Ref. 66).

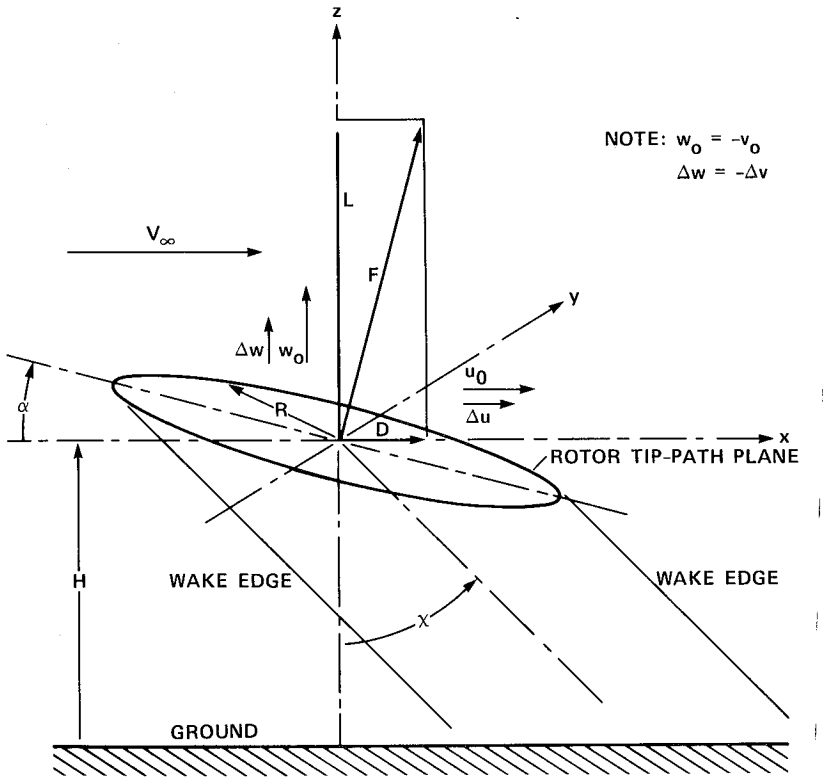

Figure 25. Rotor and wake in ground effect (from Ref. 59).

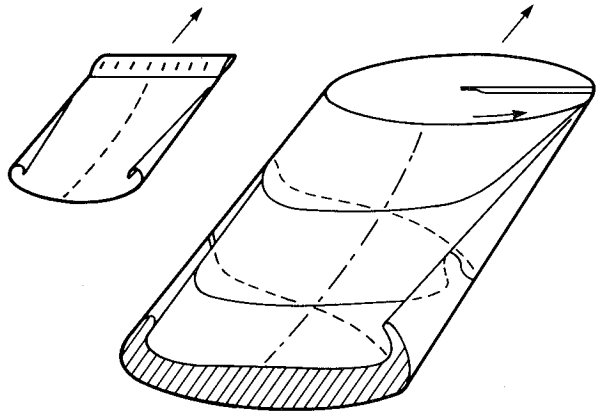

Figure 26. Schematic of rotor and fixed-wing wakes (from Ref. 77).

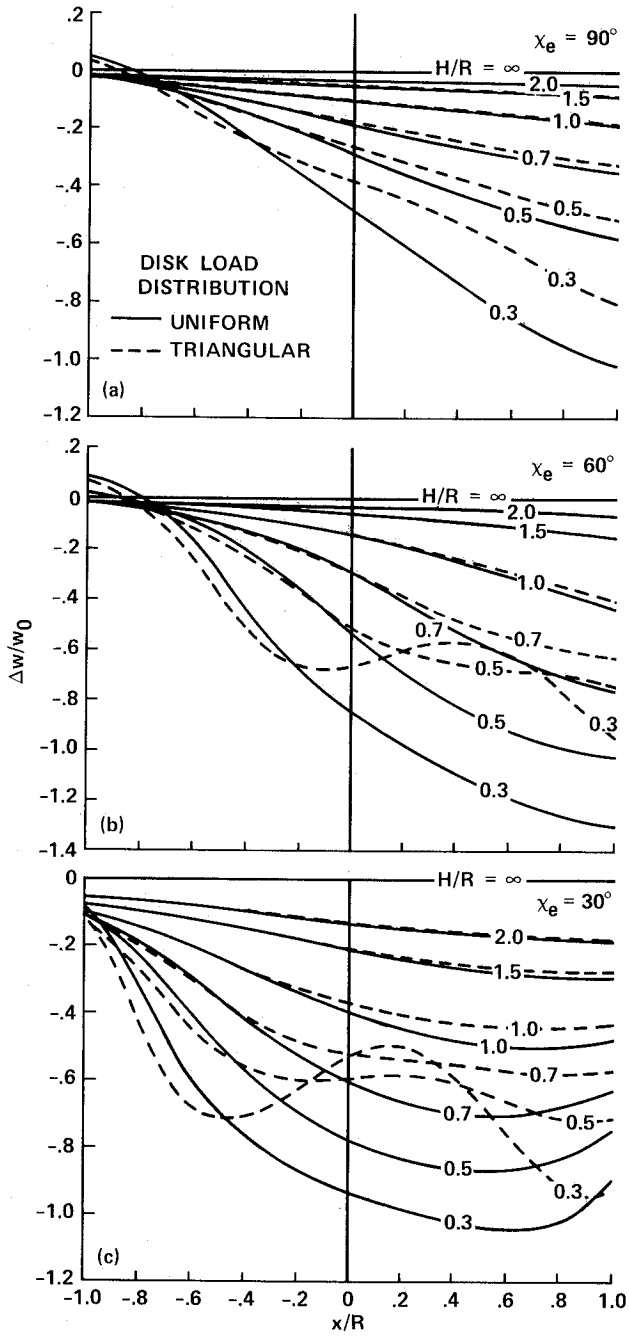

Figure 27. Distribution of the vertical component of ground-induced interference velocity over the longitudinal axis of a rotor in forward flight, $\alpha = 0°$ (from Ref. 59).

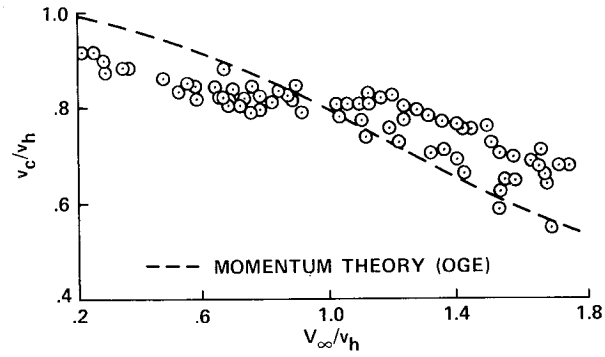

Figure 28. Constant component of induced velocity as a function of normalized advance ratio as determined from thrust measurement ($\theta_{0.75} = 9.8°$, shaft angle of attack = 0°, $A_{1c} = -1.5°$, z/R = 0.88) (from Ref. 73).

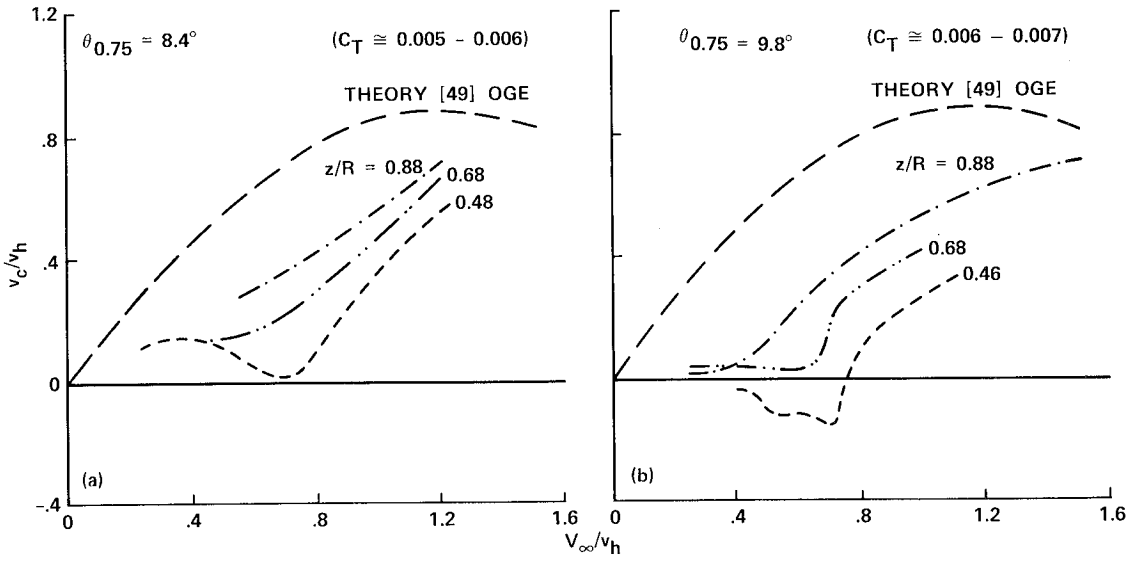

Figure 29. Normalized cosine of harmonic induced velocity as a function of normalized advance ratio and height-to-radius ratio determined from hub moment measurements (shaft angle of attack = 0°). (a) $\theta_{0.75} = 8.4°$. (b) $\theta_{0.75} = 9.8°$ (from Ref. 73).

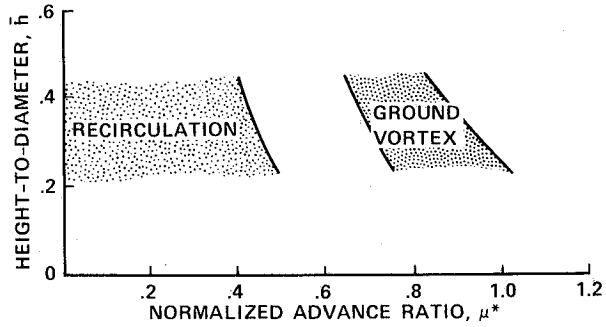

Figure 30. Boundaries for recirculation and ground vortex flow regimes determined from flow visualization studies (from Ref. 74).

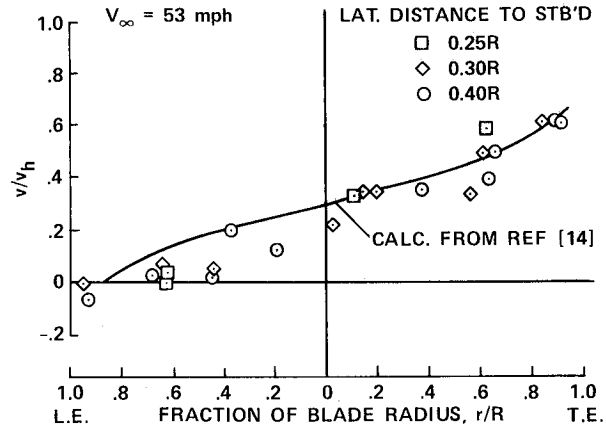

Figure 31. Comparison of calculated and measured (approximated from smoke-flow pictures) induced velocities (from Ref. 10).

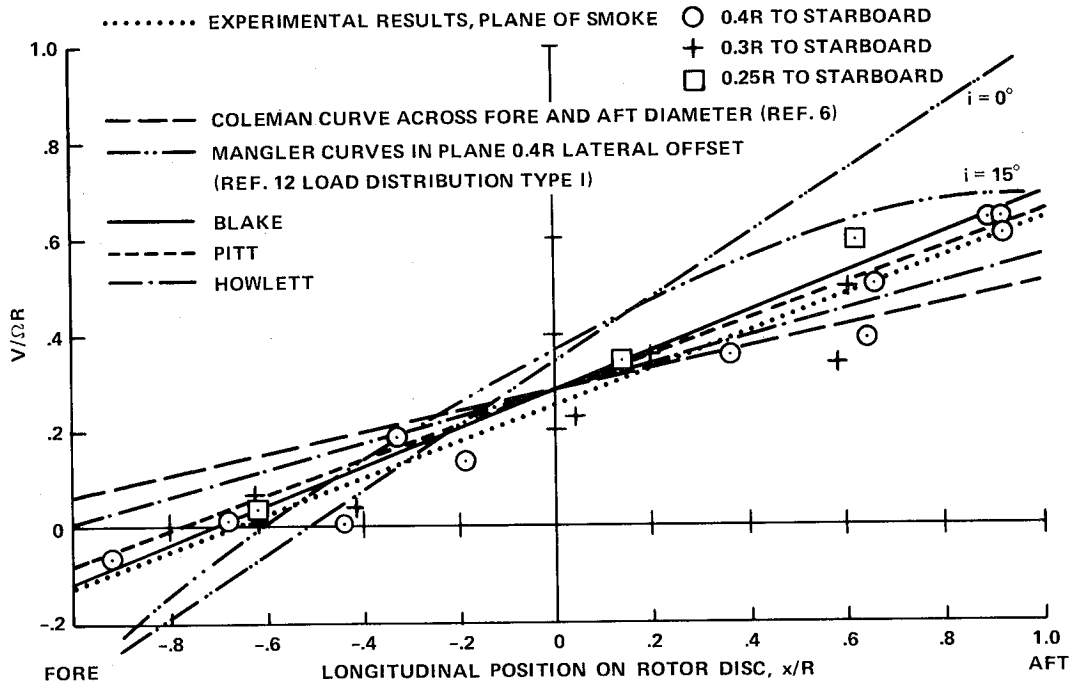

Figure 32. Comparison of calculated and measured induced velocity distributions in longitudinal plane of symmetry ($\mu = 0.167$).

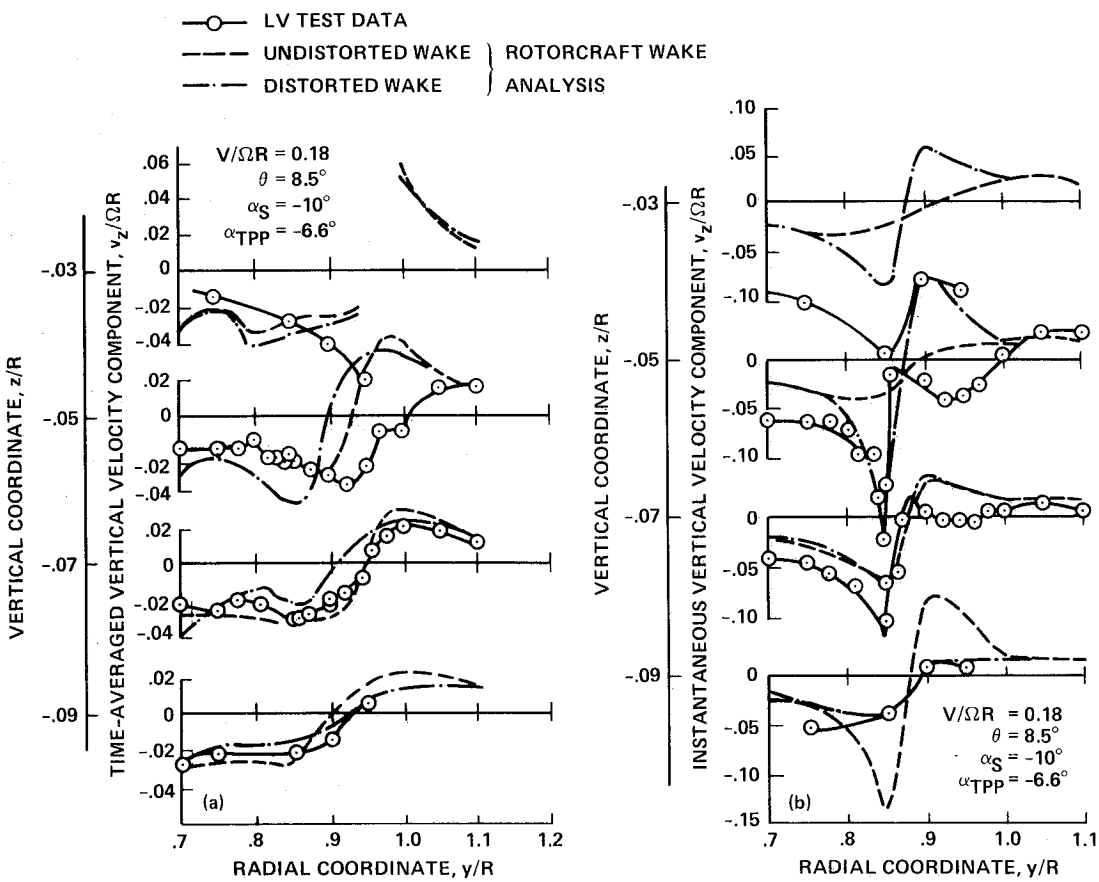

Figure 33. Calculated and measured radial distributions of vertical component of induced velocity beneath the advancing blade of a NASA model rotor. (a) Time-averaged values. (b) Instantaneous values (from Ref. 75).

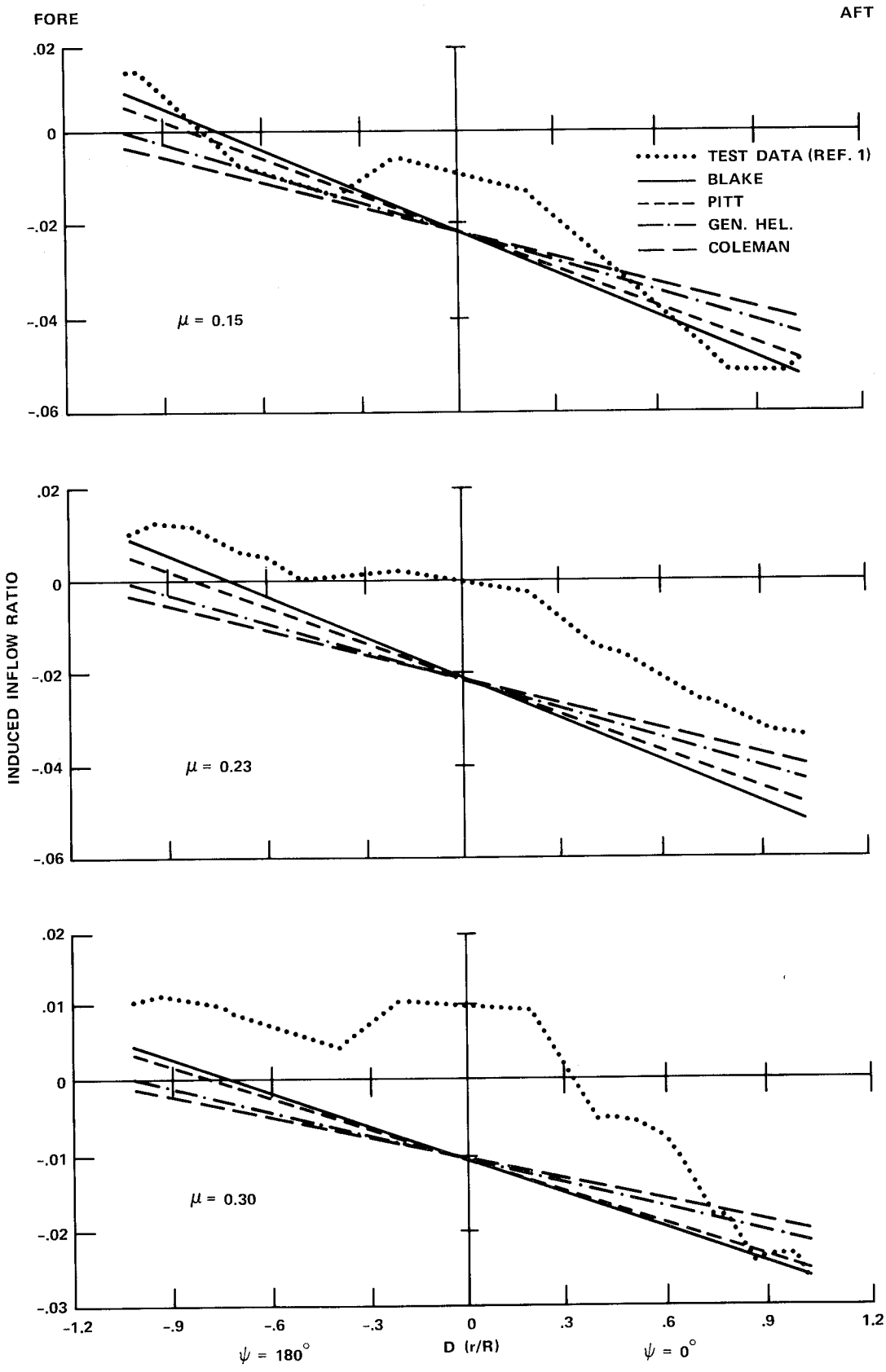

Figure 34. Comparison of calculated and measured induced inflow ratios in the longitudinal plane of symmetry at three advance ratios.

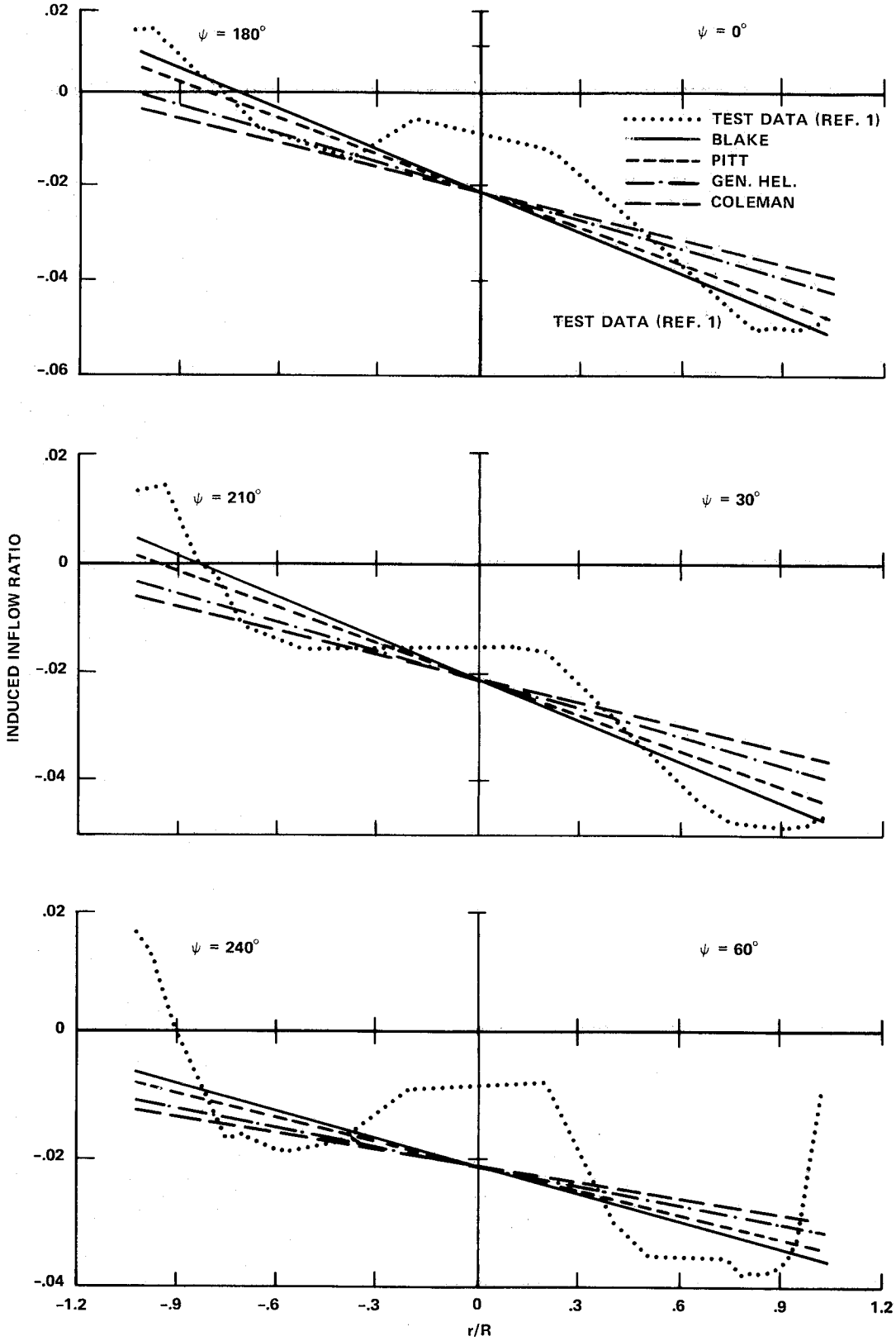

Figure 35. Comparison of measured and calculated induced inflow-ratio distributions at $\mu = 0.15$ for several azimuthal positions.

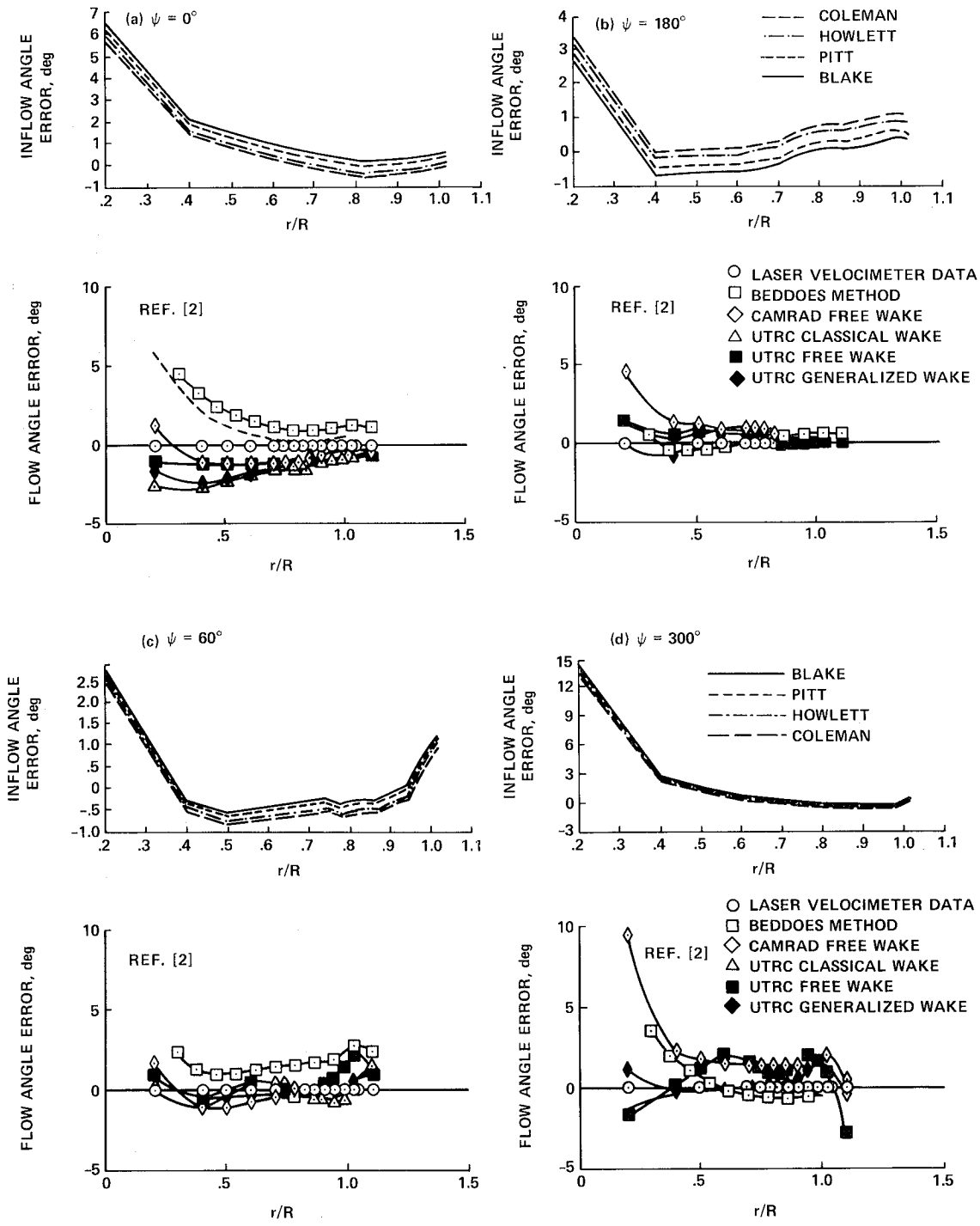

Figure 36. Comparison of inflow-angle errors calculated from simple first-harmonic inflow models with those from wake models evaluated in Ref. 2, $\mu = 0.15$. (a) $\psi = 0°$. (b) $\psi = 180°$. (c) $\psi = 60°$. (d) $\psi = 300°$.

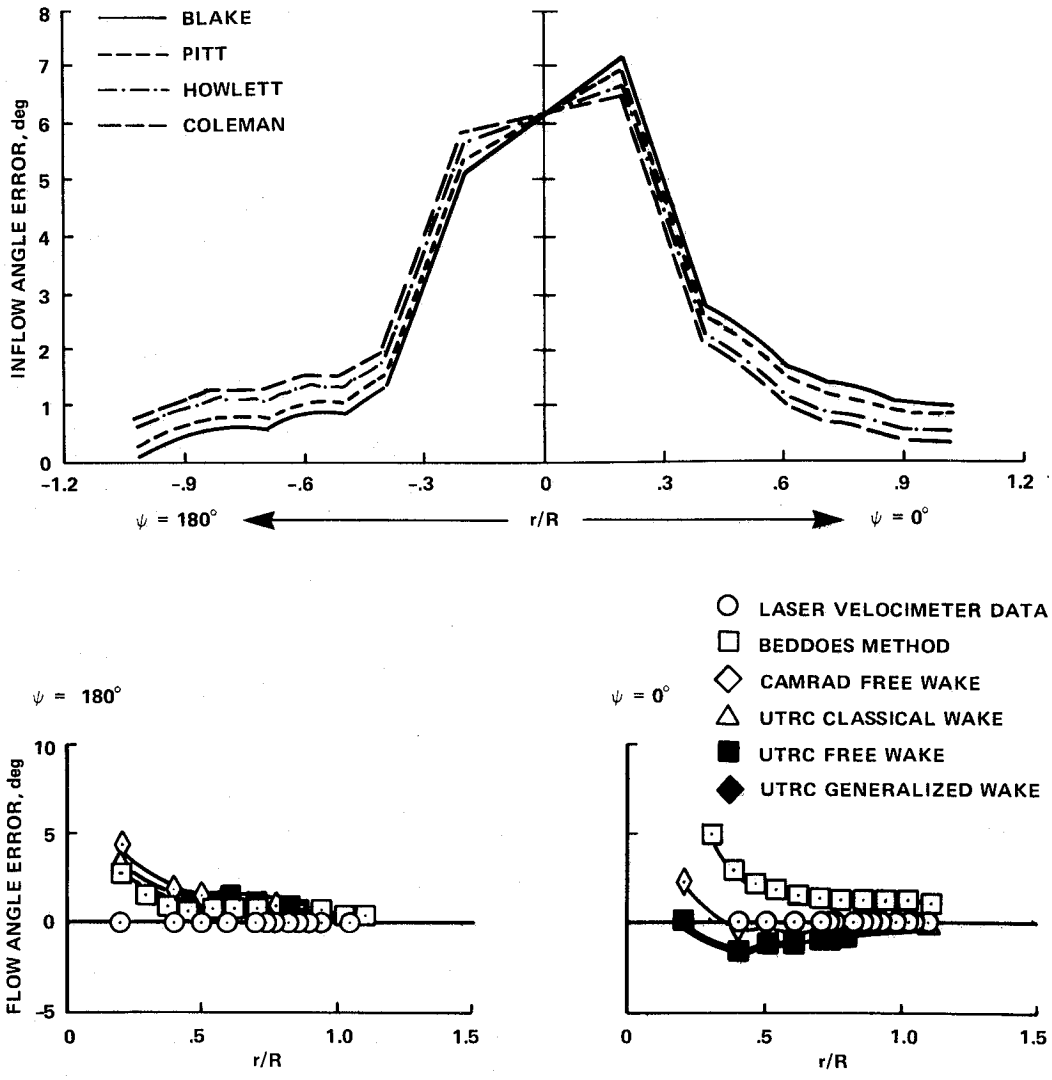

Figure 37. Comparison of inflow-angle errors calculated from simple first-harmonic inflow models with those from wake models evaluated in Ref. 2, $\mu = 0.23$.

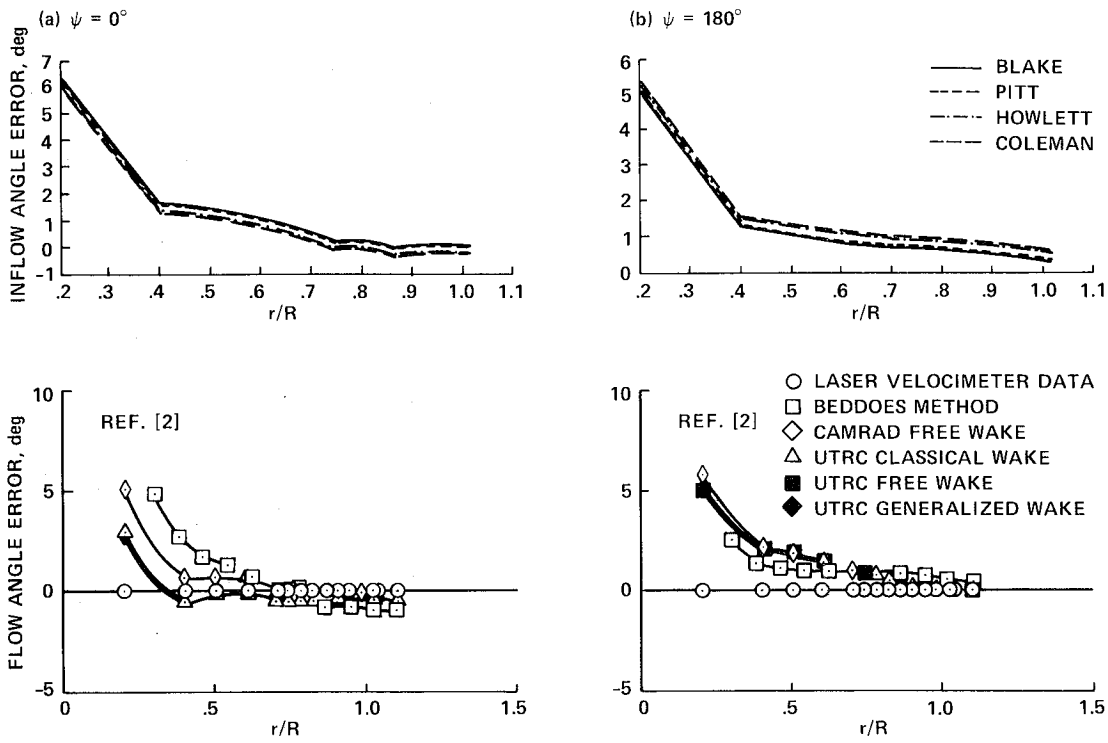

Figure 38. Comparison of inflow-angle errors calculated from simple first-harmonic inflow models with those from wake models evaluated in Ref. 2, $\mu = 0.30$. (a) $\psi = 0°$. (b) $\psi = 180°$.

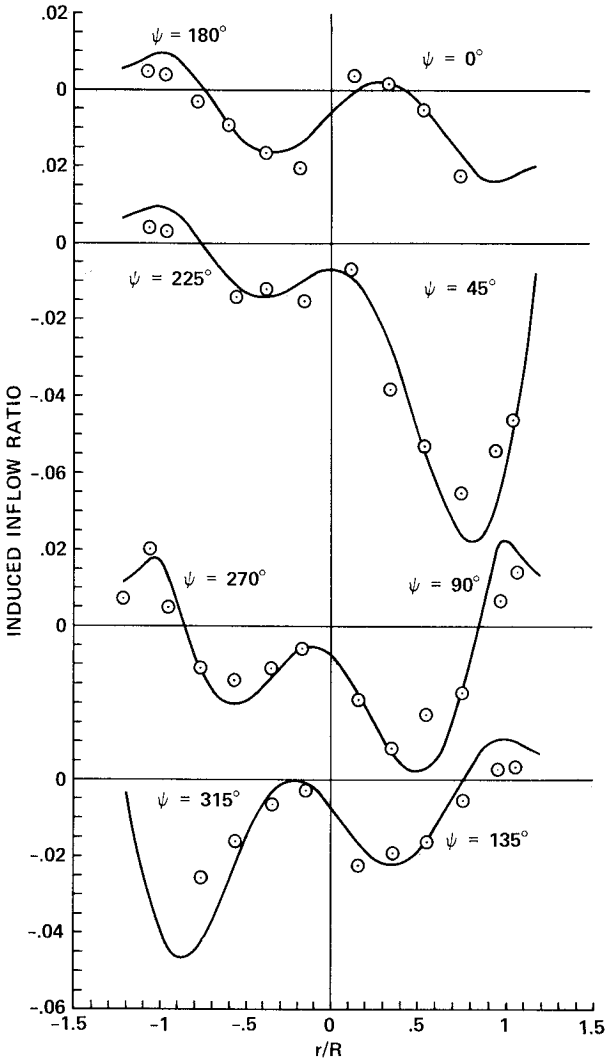

Figure 39. Correlation of Takahashi model with data from Ref. 22.

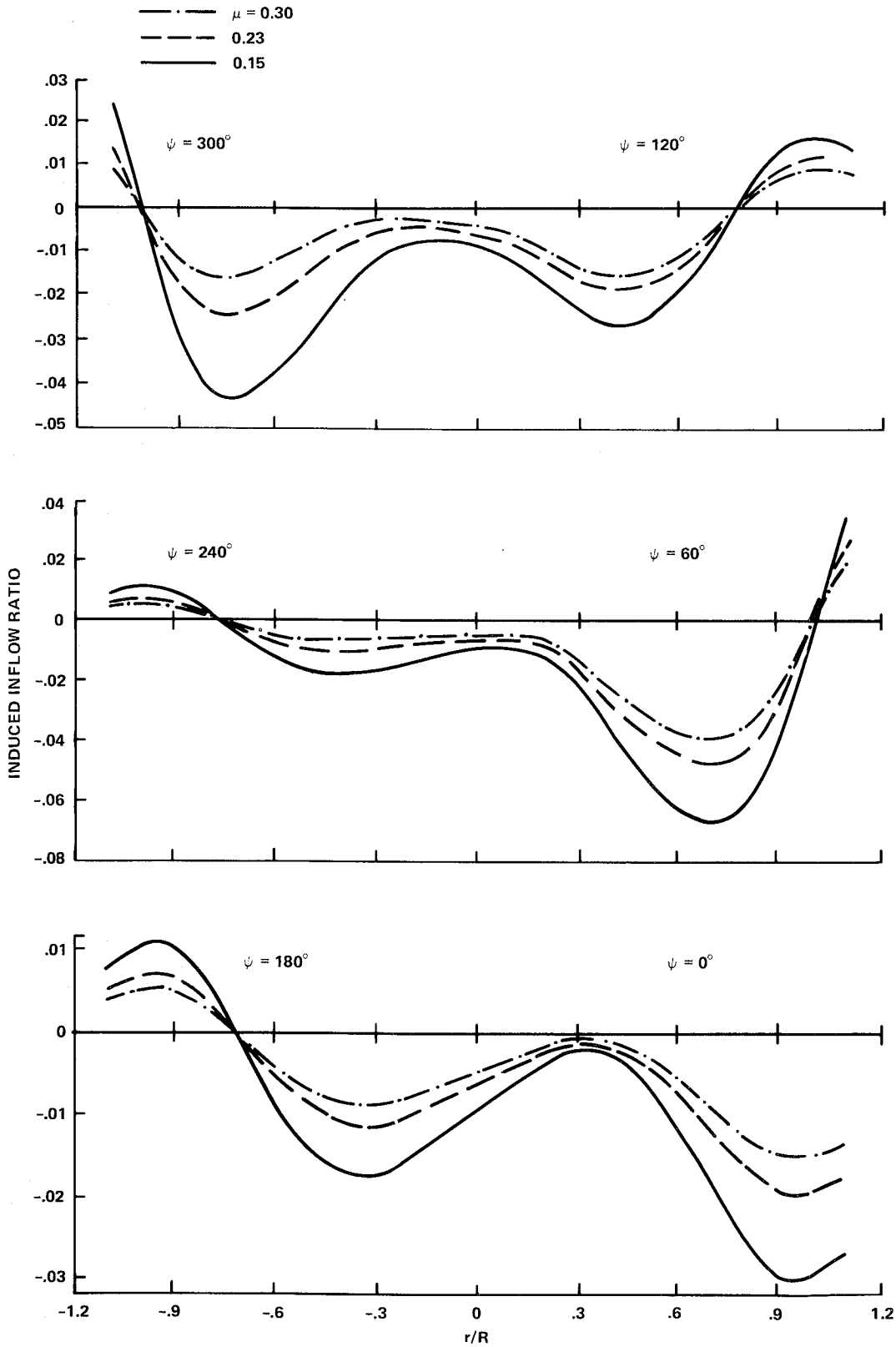

Figure 40. Induced inflow ratios calculated from Takahashi model at test conditions of Ref. 1.

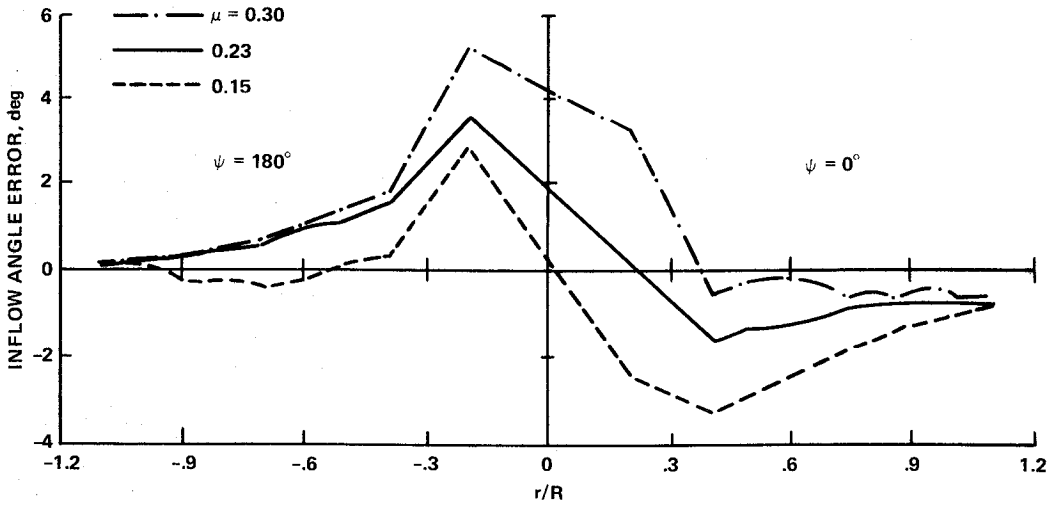

Figure 41. Induced inflow errors generated from Takahashi model in the longitudinal plane of symmetry for the three advance ratios tested in Ref. 1.

NASA
National Aeronautics and Space Administration

Report Documentation Page

1. Report No.	2. Government Accession No.	3. Recipient's Catalog No.
NASA TM-102219		

4. Title and Subtitle
A Survey of Nonuniform Inflow Models for Rotorcraft Flight Dynamics and Control Applications

5. Report Date
November 1989

6. Performing Organization Code

7. Author(s)
Robert T. N. Chen

8. Performing Organization Report No.
A-89220

10. Work Unit No.
505-61-51

9. Performing Organization Name and Address
Ames Research Center
Moffett Field, CA 94035

11. Contract or Grant No.

13. Type of Report and Period Covered
Technical Memorandum

12. Sponsoring Agency Name and Address
National Aeronautics and Space Administration
Washington, DC 20546-0001

14. Sponsoring Agency Code

15. Supplementary Notes
Point of Contact: Robert T. N. Chen, Ames Research Center, MS 211-2, Moffett Field, CA 94035
(415) 694-5008 or FTS 464-5008
This paper was originally prepared for the Fifteenth European Rotorcraft Forum, September 12-15, 1989, Amsterdam.

16. Abstract

This paper summarizes the results of a brief survey of nonuniform inflow models for the calculation of induced velocities at and near a lifting rotor in and out of ground effect. The survey, conducted from the perspective of flight dynamics and control applications, covers a spectrum of flight conditions including hover, vertical flight, and low-speed and high-speed forward flight, and reviews both static and dynamic aspects of the inflow. A primary emphasis is on the evaluation of various simple first harmonic inflow models developed over the years, in comparison with more sophisticated methods developed for use in performance and airload computations. The results of correlation with several sets of test data obtained at the rotor out of ground effect indicate that the Pitt/Peters first harmonic inflow model works well overall. For inflow near the rotor or in ground effect, it is suggested that charts similar to those of Heyson/Katzoff and Castles/De Leeuw of NACA be produced using modern free-wake methods for use in flight dynamic analyses and simulations.

17. Key Words (Suggested by Author(s))	18. Distribution Statement
Induced velocity Inflow dynamics Flight dynamics Ground effect	Unclassified-Unlimited Subject Category - 08

19. Security Classif. (of this report)	20. Security Classif. (of this page)	21. No. of Pages	22. Price
Unclassified	Unclassified	65	A04

For sale by the National Technical Information Service, Springfield, Virginia 22161